CREEP-FATIGUE MODELLING IN STRUCTURAL STEELS USING EMPIRICAL AND CONSTITUTIVE CREEP METHODS IMPLEMENTED IN A STRIP-YIELD MODEL

A Thesis

Presented in Partial Fulfilment of the Requirements for the

Degree of Master of Science

with a

Major in Mechanical Engineering

in the

College of Engineering

University of Idaho

by

Benjamin J. Andrews

December 2014

Major Professor: Gabriel Potirniche, Ph.D.

Authorization to Submit Thesis

This thesis of Benjamin Andrews, submitted for the degree of Master of Science with a Major in Mechanical Engineering and titled "Creep-Fatigue Modelling in Structural Steels using Empirical and Constitutive Creep Methods Implemented in a Strip-Yield Model," has been reviewed in final form. Permission, as indicated by the signatures and dates below, is now granted to submit final copies to the College of Graduate Studies for approval.

Major Professor:	_____ Date: _____	
	Gabriel Potirniche, Ph.D.	
Committee Members:	_____ Date: _____	
	Indrajit Charit, Ph.D.	
	_____ Date: _____	
	Robert Stephens, Ph.D.	
	_____ Date: _____	
	Gregory Donohoe, Ph.D.	
Department Administrator:	_____ Date: _____	
	John Crepeau, Ph.D.	
Discipline's College Dean:	_____ Date: _____	
	Larry Stauffer, Ph.D.	

Final Approval and Acceptance

Dean of the College of Graduate Studies:	_____ Date: _____	
	Jie Chen, Ph.D.	

Abstract

The phenomena of creep and fatigue have each been thoroughly studied. More recently, attempts have been made to predict the damage evolution in engineering materials due to combined creep and fatigue loading, but these formulations have been strictly empirical and have not been used successfully outside of a narrow set of conditions. This work proposes a new creep-fatigue crack growth model based on constitutive creep equations (adjusted to experimental data) and Paris law fatigue crack growth. Predictions from this model are compared to experimental data in two steels: modified 9Cr-1Mo steel and AISI 316L stainless steel.

Modified 9Cr-1Mo steel is a high-strength steel used in the construction of pressure vessels and piping for nuclear and conventional power plants, especially for high temperature applications. Creep-fatigue and pure creep experimental data from the literature are compared to model predictions, and they show good agreement.

Material constants for the constitutive creep model are obtained for AISI 316L stainless steel, an alloy steel widely used for temperature and corrosion resistance for such components as exhaust manifolds, furnace parts, heat exchangers and jet engine parts. Model predictions are compared to pure creep experimental data, with satisfactory results.

Assumptions and constraints inherent in the implementation of the present model are examined. They include: spatial discretization, similitude, plane stress constraint and linear elasticity. It is shown that the implementation of the present model had a non-trivial impact on the model solutions in 316L stainless steel, especially the spatial discretization.

Based on these studies, the following conclusions are drawn:

1. The constitutive creep model consistently performs better than the Nikbin, Smith and Webster (NSW) model for predicting creep and creep-fatigue crack extension.

2. Given a database of uniaxial creep test data, a constitutive material model such as the one developed for modified 9Cr-1Mo can be developed for other materials.
3. Due to the assumptions used to develop the strip-yield model, model predictions are expected to show some scatter, especially in some situations.

Several areas of future research are proposed from these conclusions:

1. Alternative methods for predicting fatigue crack growth, especially a constitutive fatigue crack growth model,
2. Continued development of new material models and refinement the existing ones, and
3. Implementation of the present creep-fatigue model as a user-defined subroutine in a finite element solver.

Acknowledgements

The author would like to gratefully acknowledge the assistance of Dr. Gabriel Potirniche in helping to select this topic and invaluable feedback and guidance throughout the research project.

Dedication

I would like to thank my wonderful wife, Lynn Andrews, for tireless support through many late nights and long weekends of research. Her dedication and moral support were essential to my successful completion of this research project.

Table of Contents

List of Figures

List of Tables

Chapter 1 – Literature Review

1.1. INTRODUCTION

Engineering analysis has historically considered either a constant (steady) load using the techniques of fracture mechanics or a cyclic (time varying) load using the techniques of fatigue analysis. Actual service conditions for many components in the energy and aerospace industries (such as pressure vessels, piping, turbines, etc.) are typically a combination of these types of loads. This study will examine two steels commonly used in high temperature environments: modified 9Cr-1Mo steel and AISI 316L stainless steel.

In the 1960s, a class of high-strength, high-chromium steels, designated 9Cr-1Mo, was designed for fossil fuel power plants. As power plant operating temperatures increased, it became clear that the creep performance of 9Cr-1Mo steel was limited. Modified 9Cr-1Mo steel is a ferritic-martensitic steel developed from 9Cr-1Mo steel by adding Niobium and Vanadium. These elements add superior creep resistance to the high strength and corrosion resistance of 9Cr-1Mo steel. These properties make modified 9Cr-1Mo steel a popular material choice for pressure vessels, piping, and steam generators in both nuclear and fossil fuel power plants. Service conditions in these applications are typically an aqueous environment, temperatures of 500-700°C with thermal stresses, which can have high magnitude. Recently, modified 9Cr-1Mo steel has been investigated by researchers around the world for potential applications in the next generation of nuclear power plant designs.

AISI 316L stainless steel is a low-carbon, austenitic stainless steel, which was developed based on the other AISI 300 stainless steels (e.g. 304). AISI 316L stainless steel provides superior corrosion and pitting resistance in acidic and saline environments, as well as high creep resistance at high temperature and superior rupture and tensile strength at high temperatures. These characteristics make 316L stainless steel an attractive choice for a diverse field of applications including jet engine parts, heat exchangers, surgical instruments, cutlery and jewelry. Typical

service conditions for this material are as diverse as its applications. In applications where creep-fatigue would be a concern (i.e., jet engines, petro-chemical piping, furnaces, etc.), service conditions typically involve an environment with variety of corrosive agents, temperatures of 500-700°C and a combination of mechanical and thermal stresses.

The importance of analyzing the combination of fatigue and fracture damage is highlighted by conditions such as high temperature and corrosive chemistry. As demand for cleaner energy and more efficient power plants drives higher operating temperatures and more refined chemistry, models that can successfully predict damage evolution and failure due to combined steady and cyclic loads are essential. Other researchers have studied aspects of this problem using a variety of approaches. This chapter will examine this previous research to inform the development of the present model.

1.2. NOMENCLATURE

The following terms are used throughout this thesis and are defined here for convenience.

a – Crack length

$\dot{a}$ – Creep crack extension rate

C^* – A crack tip contour integral, analogous to J integral, empirically correlated to creep crack extension rate

k_Λ – Empirical correlation constant

W – Specimen width (half width for center cracked plates and for double edge notched tension specimens)

$\Delta\sigma$ – stress range for a cyclic stress event

ΔK – stress intensity factor range for a cyclic stress event

$\dot{\varepsilon}_s$ – secondary (or minimum) creep strain rate

ρ_m – The density of the mobile dislocations in a material

σ – applied stress

σ_0 – flow stress

da/dN – Crack growth rate due to fatigue

HRR stress/strain field – Crack tip stress or strain field described by Hutchinson, Rice and Rosengren

NSW model – A creep crack extension model developed by Nikbin, Smith and Webster using the crack tip parameter C*

True plastic strain – The difference between true total strain and true elastic strain

1.3. STRIP YIELD MODEL

Potirniche proposed a model for predicting primary and secondary creep [1] using Dugdale's strip yield model [2]. This method employed Norton's power law to predict creep strain, and used the strip yield model to accumulate crack tip damage by calculating a decline in the flow stress (average of the yield stress and ultimate tensile strength). The model compared favorably to test data available in the literature [3, 4].

Newman used a modified strip yield model to predict fatigue crack growth, with some success [5]. This model included a formulation for yield strips in the plastic wake and a stress intensity factor (SIF) solution that accounted for crack growth rate retardation due to plasticity-induced crack closure (PICC). The plastic wake yield strips used a simple, displacement-based formulation (similar to early finite element method contact methods) with the strip-yield model and an elastic-perfectly-plastic material model to predict adjustments to the SIF (see Figure 1.1).

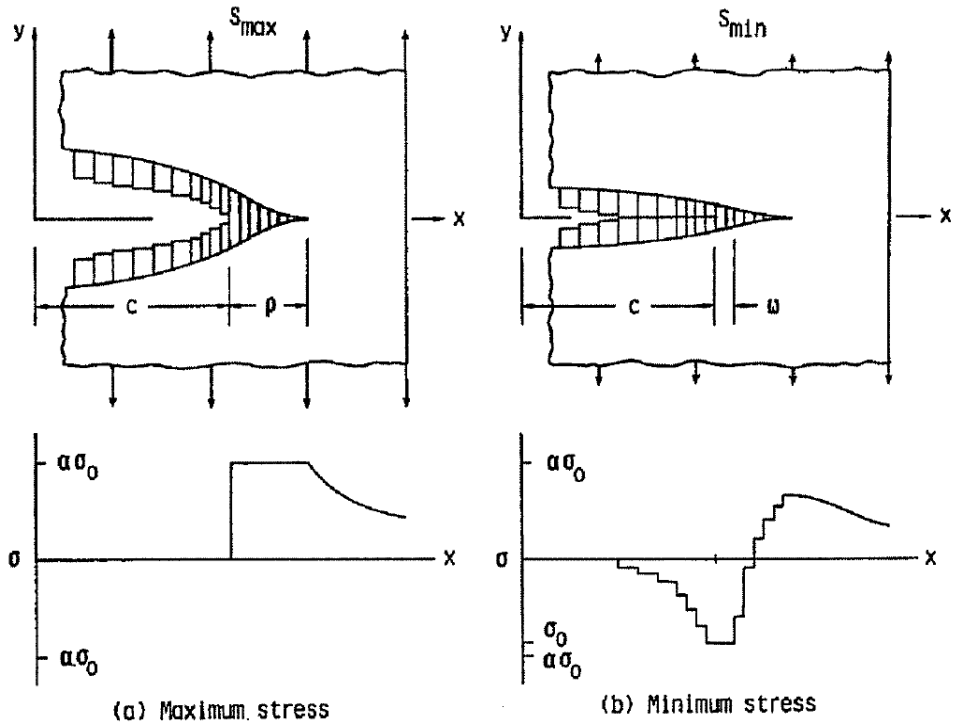

Fig. 1.1 – Schematic of the strip-yield model with a plasticity-induced crack closure model.

This method showed some promising results, however, it requires a robust test program to calibrate the model before it can be used to make predictions [6].

1.4. MATERIALS

Modified 9Cr-1Mo steel (designated by the ASTM as Grade 91 steel) is a high strength alloy steel designed for high resistance creep, corrosion and stress corrosion cracking [7]. Since its development in the 1970s, modified 9Cr-1Mo steel has been a popular choice for components serving in petrochemical plants, sodium cooled fast reactors (especially in steam generator components, where stress corrosion cracking is a concern [8]), thermal power plants, nuclear power plants and fast breeder reactors [7]. These characteristics, in addition to a high resistance to the detrimental effects of large doses of radiation, also make modified 9Cr-1Mo steel appealing to

designers of fusion reactors [9]. AISI 316L stainless steel is a corrosion and fatigue resistant steel. It has long been used for a variety of applications such as nuclear power, chemistry, aerospace, food processing and tools [10]. More recently 316L has become a popular material choice for biomedical applications due to its high fatigue strength and ductility [10].

1.5. EMPIRICAL CREEP MODEL

Nikbin, Smith and Webster proposed a model for creep crack extension using the crack tip parameter C*, known as the NSW model [11, 12]. The parameter *C** is analogous to the J-integral proposed by Hutchinson, Rice and Rosengren (HRR) [13, 14] to characterize non-linear elastic material behavior [15, 16]. *C** has been shown to predict well creep crack extension in HRR stress-strain fields (i.e., stress-strain fields in which the relationship between stress and strain is elastic and non-linear) [11, 17, 18]. The NSW model is often presented as a power law expression (analogous to the Paris law for fatigue crack growth) where the constant and power are derived from the equations for the HRR stress/strain fields [19].

HRR stress-strain fields have been shown to accurately predict crack tip stress fields in many cases [13, 20]. Figure 1.2 shows crack tip stress fields predicted by HRR.

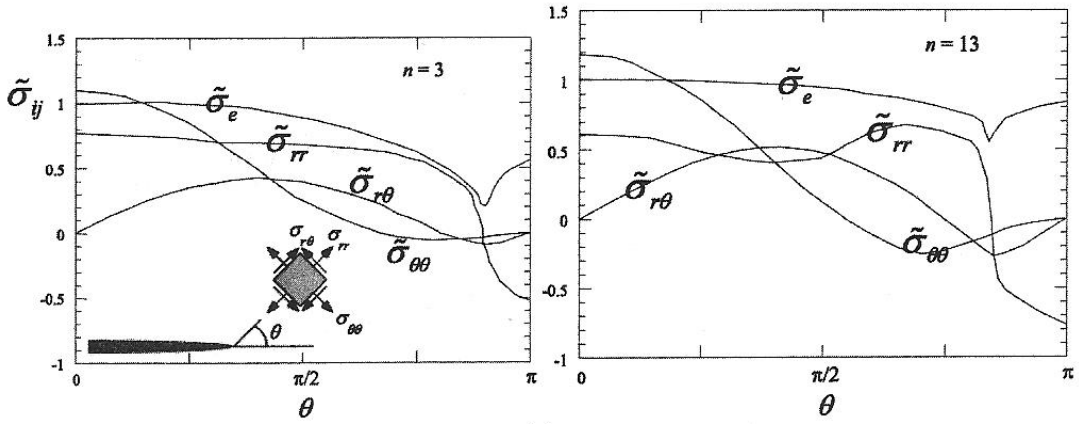

Fig. 1.2 – Non-dimensional HRR crack tip stress fields in plane stress as function of angular position [20]. In this figure n refers to the strain hardening exponent.

HRR stress fields do not correlate well to crack tip stress fields in cases of large deformations (see Figures 1.3 and 1.4). Furthermore, they are only strictly valid for monotonically increasing loads, since the unloading path is different for elastic-plastic and elastic, non-linear materials (see Figure 1.5). This is not a concern for creep modelling though it does require special consideration when preforming fatigue crack growth predictions.

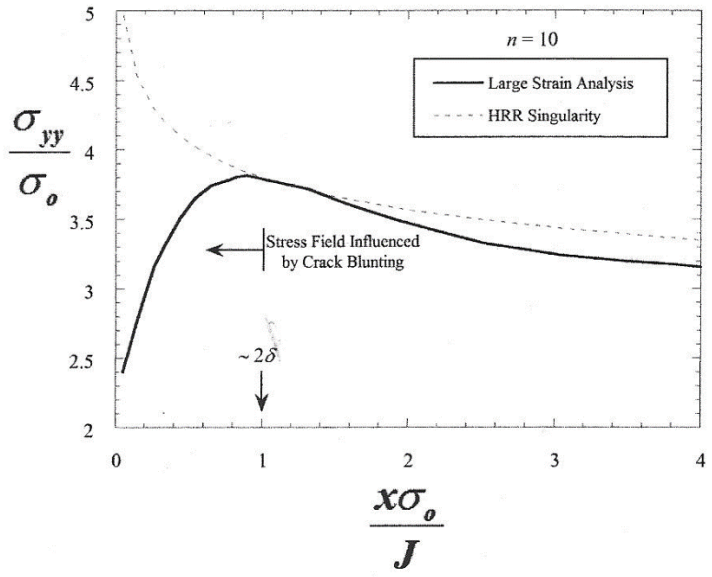

Fig. 1.3 – Crack tip stress fields predicted by HRR compared to finite element analysis in a case of large deformation. Note that $\sigma_{yy} = \sigma_{\theta\theta}$ when $\theta = 0$.

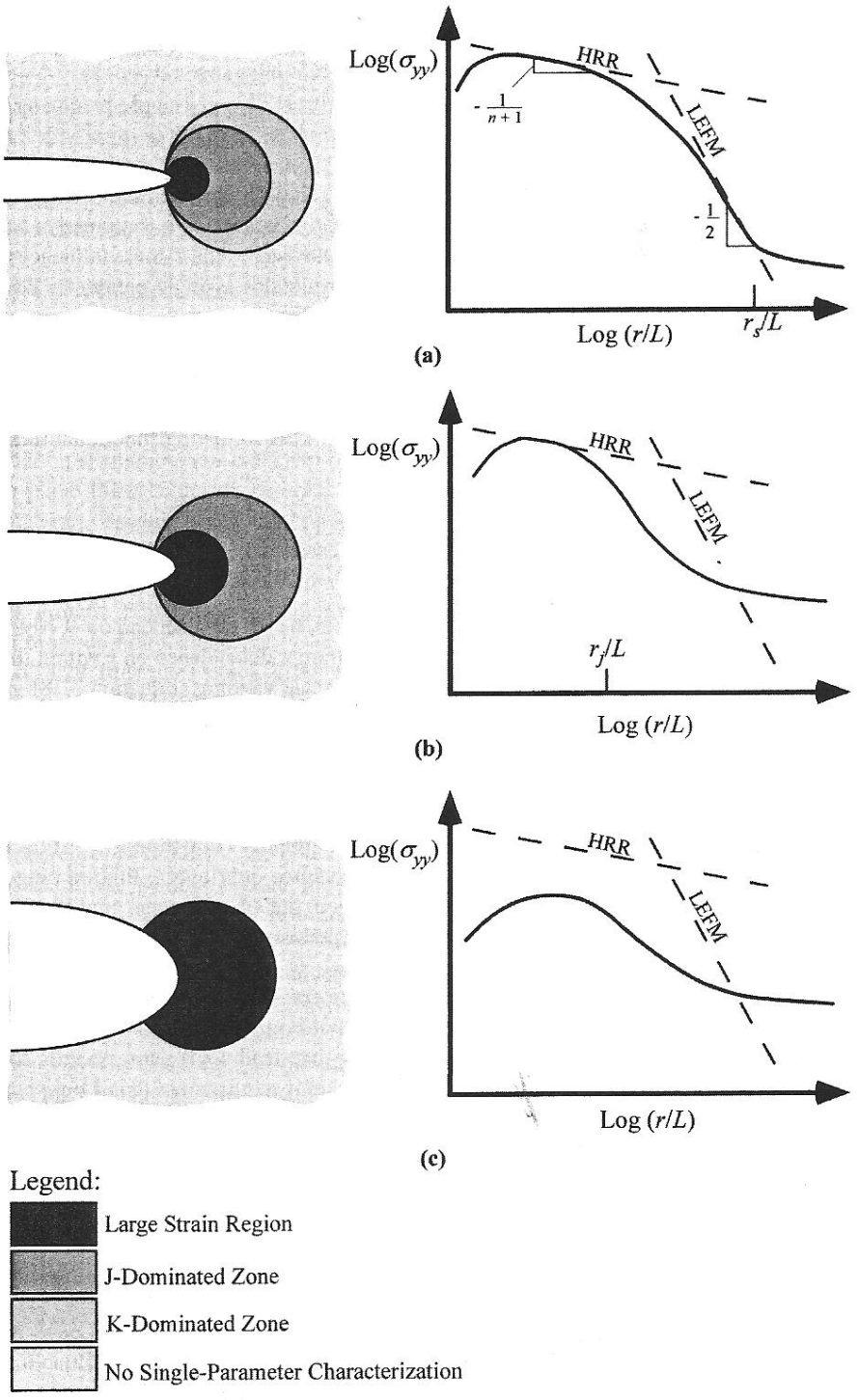

Fig. 1.4 – Effect of plasticity on crack tip stress fields in (a) small scale yielding (linear elastic), (b) elastic-plastic and (c) large deformation. Note that, in this figure, r is the distance from the crack tip and L is the plastic zone size.

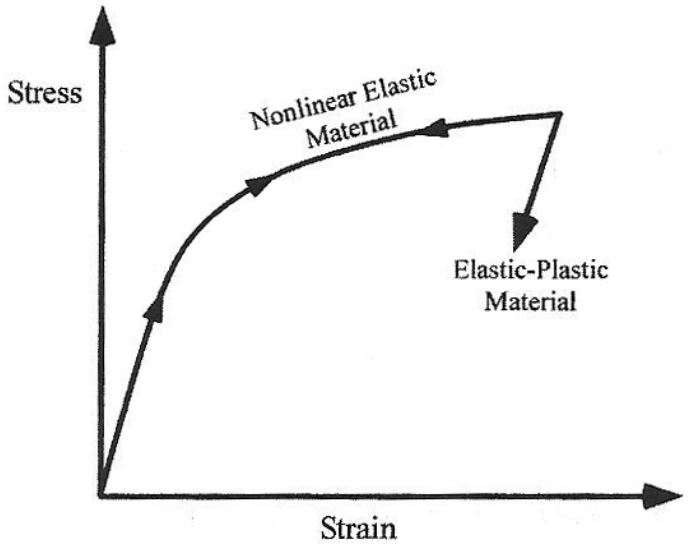

Fig. 1.5 – Unloading paths for elastic-plastic and elastic, non-linear materials.

Narasimhachary and Saxena conducted creep-fatigue crack growth experiments in modified 9Cr-1Mo [21] and compared it to predictions using a C^*-based model. They found that the predictions from this model were more accurate than predictions based on ΔK and suggested the model predictions could be improved by conducting load-line displacements tests for use in calculating C^* [21]. Wasmer, Nikbin and Webster compared the results of creep-fatigue crack growth experiments in 316L stainless steel to predictions from a modified NSW model [22]. C^* was estimated using the reference stress method and Wasmer et. al. found that the accuracy of the analytical predictions were strongly dependent on the reference stress correlation used.

1.6. CONSTITUTIVE CREEP MODEL

Basirat et. al. proposed a constitutive creep model based on the fundamental mechanisms that drive the creep phenomena, such as dislocation density and mobility [23]. This model was shown to agree well with uniaxial creep data in modified 9Cr-1Mo steel. The model is based on Orowan's equation (a primary and secondary constitutive creep correlation) and was modified to

predict tertiary creep using damage mechanics. Tertiary creep begins with the initiation of a crack which extends until failure. By considering the micro-mechanical phenomena that cause crack initiation and extension, damage terms were introduced to Orowan's equation that were shown to predict all creep stages quite accurately.

1.7. CONCLUSION

Although some researchers have studied creep and fatigue crack growth interactions [24-26], a successful model with applications beyond a specific combination of load sequence and material remains elusive.

Some success has been obtained in the past using a strip-yield model to predict crack tip stresses for fatigue crack growth and creep crack extension. [1, 5] Due to the extensive test data required to calibrate Newman's strip-yield model for fatigue crack growth with PICC, crack closure will not be modeled in the present implementation of the strip-yield model. Fatigue crack growth will be modeled using the classic Paris law formulation for linear elastic fracture mechanics.

Both the NSW model and the constitutive creep model will be implemented with the strip yield model. These methods will be used to predict creep and creep-fatigue crack extension in test specimens. These predictions can be compared to test results in order to evaluate these methods and the integration with the fatigue crack growth model.

1.8. REFERENCES

[1] Potirniche GP. A Numerical Strip-Yield Model for the Creep Crack Incubation in Steels. J. of ASTM International. 2012;9(3):1-13.

[2] Dugdale DS. Yielding of Steel Sheets Containing Slits. J. Mechanics & Phys. of Solids. 1960;8:100–4.

[3] Ewing DJF. Strip Yield Models of Creep Crack Incubation. International J. of Fracture, 1978;14:101–17.

[4] Haigh JR. The Mechanisms of Macroscopic High Temperature Crack Growth. Part I: Experiments on Tempered Cr-Mo-V Steels. Material Science Engineering. 1975;20:213–23.

[5] Newman, Jr. JC. A Crack Closure Model for Predicting Fatigue Crack Growth under Aircraft Spectrum Loading. Methods and Models for Predicting Fatigue Crack Growth under Random Loading, ASTM STP 748. Chang JB, Hudson CM, Eds. Philadelphia: American Society for Testing and Materials; 1981:53-84.

[6] Smith KV. Application of the dissipated energy criterion to predict fatigue crack growth of Type 304 stainless steel following a tensile overload. Engineering Fracture Mechanics. 2011;78:3183-95.

[7] Ennis PJ, Czyrska-Filemonowicz A. Recent advances in creep-resistant steels for power plant applications. Sadhana. 2003;28(3&4):709-30.

[8] Christopher J et. al. Continuum Damage Mechanics Approach to Predict Creep Behavior of Modified 9Cr-1Mo Ferritic Steel at 873K. In: Chetal, SC, editor. 6th International Conference on Creep, Fatigue and Creep-Fatigue Interaction 2012; 22-25 January 2012; Kalpakkam, India. Red Hook, NY: Curran Associates, Inc.; c2013. p. 798-804.

[9] Giordana MF et. al. Microstructure evolution during cyclic tests on EUROFER 97 at room temperature TEM observation and modelling. Materials Science and Engineering A. 2012;550:103-11

[10] Auricchio F, Constantinescu A, Scalet G. Fatigue of 316L stainless steel notched μm-size components. International J. of Fatigue. 2014;68:231-47.

[11] Webster GA, Ainsworth RA. High Temperature Component Life Assessment. First ed. London: Chapman & Hall; 1994.

[12] Nikbin KM, Smith DJ, Webster GA. An engineering approach to the prediction of creep crack growth. J. Engineering Material Technology. 1986;108:186–91.

[13] Hutchinson JW, Singular Behavior at the End of a Tensile Crack in a Hardening Material. J. Mechanics & Phys. of Solids. 1968;16:13-31.

[14] Rice JR, Rosengren GF. Plane Strain Deformation near a Crack Tip in a Power-Law Hardening Material. J. Mech. Phys. Solids. 1968;16:1-12.

[15] Vainshtok VA, Baumshtein MV, Makovetskaya IA, Kramarenko IV. Creep Crack Growth Laws in Heat Resistant Steels. Engineering Fracture Mechanics. 1991;40(6):1147-63.

[16] Rice JR. Mathematical analysis in the mechanics of fracture. In: Liebowitz, H, editor. Treatise on fracture. Vol. 2, New York, NY: Academic Press; 1968.

[17] Brust FW, Majumdar BS. Load History Effects on Creep Crack Growth. Engineering Fracture Mechanics, 1994;49(6):809-37.

[18] Saxena A. Creep Crack Growth in High Temperature Ductile Materials. Engineering Fracture Mechanics. 1991;40(4/5):721-36.

[19] Yatomi, M., Nikbin, K. M., O'Dowd, N. P., 2003, "Creep crack growth prediction using a damage based approach," International Journal of Pressure Vessels and Piping, 80, pp. 573–583.

[20] Anderson TL. Fracture Mechanics: Fundamentals and Applications. Third ed. Boca Raton (FL): CRC Press; 2005.

[21] Narasimhachary SB, Saxena A. Crack growth behavior of 9Cr-1Mo (P91) steel under creep–fatigue conditions. International J. of Fatigue. 2013;56:106–13.

[22] Wasmer K, Mikbin KM, Webster GA. Influence of reference stress formulae on creep and creep-fatigue crack initiation and growth prediction in plate components. International J. Pressure Vessels and Piping. 2010;87:447-56.

[23] Basirat M, Shrestha T, Potirniche GP, Charit I, Rink K. A study of the creep behavior of modified 9Cr–1Mo steel using continuum-damage modeling. International J. of Plasticity. 2012;37:95–107.

[24] Narasimhachary SB, Saxena A. Crack growth behavior of 9Cr-1Mo (P91) steel under creep–fatigue conditions. International J. of Fatigue. 2013;56:106–13.

[25] Granacher, J., Klenk, A., Tramer, M., Schellenberg, G., Mueller, F., Ewald, J., 2001, "Creep fatigue crack behavior of two power plant steels," International Journal of Pressure Vessels and Piping, 78, pp. 909-920.

[26] Henaff G, Odemer G, Benoit G, Koffi E, Journet B. Prediction of creep–fatigue crack growth rates in inert and active environments in an aluminum alloy. International Journal of Fatigue. 2009;31:1943–51.

Chapter 2 – Explicit and Implicit Lifetime Assessment Methods under Combined Creep and Fatigue Loads Using a Strip Yield Model and Applications to Modified 9Cr-1Mo Steel

2.1. INTRODUCTION

This chapter discusses the development of two creep-fatigue lifetime assessment methods: an explicit, empirical model and an implicit, constitutive model. Since modified 9Cr-1Mo steel is a commonly used steel for high temperature applications and material properties for this steel are readily available in the literature, these models will be used to predict failure in modified 9Cr-1Mo. These predictions will be compared to experimental data so that the relative strengths and limitations of each model may be examined.

2.2. THEORY

2.2.1. MODEL OVERVIEW

In a cracked component subjected to combined cyclic and steady loads over a differential time interval *dt*, the rate of change of the crack length with time, da/dt, can be expressed [1]:

$$\frac{da}{dt} = \left(\frac{da}{dt}\right)_{time} + \left(\frac{da}{dt}\right)_{cycle} \tag{2.1}$$

where $\left(\frac{da}{dt}\right)_{time}$ is the rate of crack extension due to creep and $\left(\frac{da}{dt}\right)_{cycle}$ is the rate of crack extension due to fatigue.

Equation (2.1) may be written:

$$\frac{da}{dt} = \frac{da}{dN}\frac{dN}{dt} + \frac{da}{dt} \tag{2.2}$$

where $\frac{dN}{dt}$ is the frequency of the cyclic load.

Equation (2.2) assumes that creep damage and fatigue damage are independent phenomena, and thus there is no interaction between them. However, it has been shown that there is an interaction between the phenomena which is non-trivial in some cases [2]. For the present model, it is assumed that the creep–fatigue interaction component of the crack growth rate is the creep crack growth rate due to the stress applied during cyclic loading, or:

$$\left(\frac{da}{dt}\right)_{interaction} = \left(\frac{da}{dt}\right)_{\sigma_m} \tag{2.3}$$

where σ_m is the mean applied stress during a cyclic stress event.

Combining Equations (2.2) and (2.3), the rate of change in crack length $\dot{a}$, becomes:

$$\dot{a} = \left(\frac{da}{dN}\frac{dN}{dt}\right)_{cycle} + \left(\frac{da}{dt}\right)_{time} + \left(\frac{da}{dt}\right)_{\sigma_m} \tag{2.4}$$

2.2.2. Implementation of the Strip-Yield Model

The present model predicts secondary creep using the methodology described in [3], which relies on strip-yield modeling. The strip-yield model uses the elastic stress intensity factor, *K*, to predict the size of the plastic zone (ρ) at the crack tip [4] assuming elastic-perfectly plastic material behavior. The crack tip plastic zone (creep process zone in the present model) for a center crack in a Middle-Tension specimen is modeled by creating an equivalent crack in an infinite body of length *d* (Figure 2.1) such that:

$$d = a + \rho \tag{2.5}$$

The equivalent crack is loaded with the remote stress, σ, and the plastic zone is loaded in compression with the flow stress, σ_0, of the material. The plastic zone size is the length ρ required to eliminate the singularity of the stress intensity factor from the remote stress at the end of the process zone:

$$K_{I\sigma} + K_{I0} = 0 \tag{2.6}$$

where $K_{I\sigma}$ is the stress intensity factor from the remote stress and K_{I0} is the stress intensity factor from the crack tip flow stress.

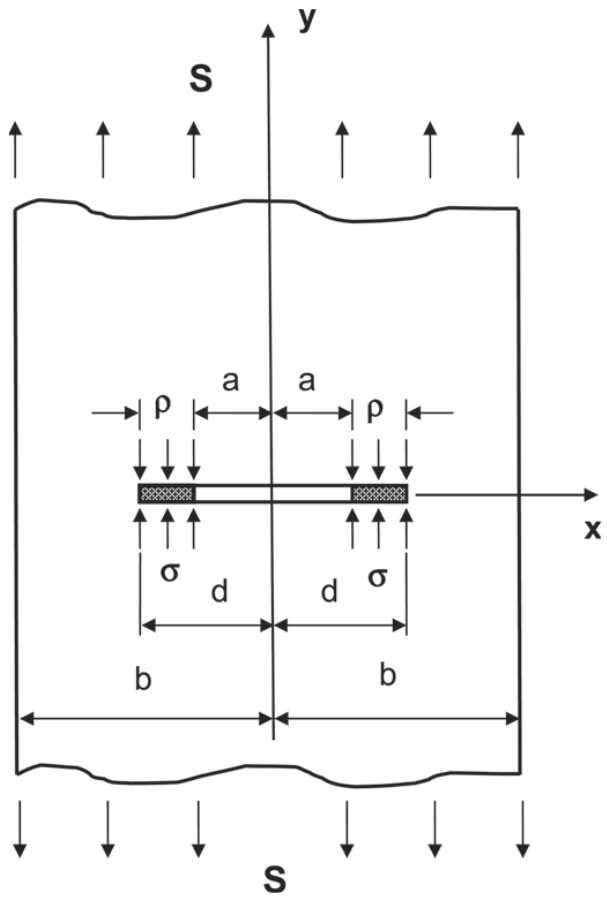

Fig. 2.1 – Schematic of the strip-yield model for a finite width center-cracked tension specimen.

The handbook [5] solution to this equation for a crack in an infinite body is:

$$\rho = a\left(sec\frac{\pi\sigma}{2\sigma_0}\right) \tag{2.7}$$

Accounting for the finite width in a center cracked plate, the plastic zone size becomes [3]:

$$\rho = \frac{2b}{\pi} sin^{-1}\left(sin\frac{\pi a}{2b} sin\frac{\pi\sigma}{2\sigma_0}\right) - a \tag{2.8}$$

where b is half the plate width.

In a strip-yield methodology, the creep process zone is discretized into "strips" and Equation (2.6) can then be solved for the displacement of each discretization strip (see [3] for details).

$$V_i = \sigma f(x_i) + \sigma_0 \sum_{j=1}^{n} g(x_i, x_j) \tag{2.9}$$

$$f(x_i) = \frac{2}{E'}\sqrt{\left(d^2 - x_i^2\right) sec\frac{\pi d}{2b}} \tag{2.10}$$

$$g\left(x_i, x_j\right) = G\left(x_i, x_j\right) + G\left(x_i, -x_j\right) \tag{2.11}$$

$$\begin{aligned} G\left(x_i, x_j\right) = \frac{2}{E'}\Bigg[&(b_2 - x_i)\, cosh^{-1}\frac{d^2 - b_2 x_i}{d|x_i - b_2|} - (b_1 - x_i)\, cosh^{-1}\frac{d^2 - b_1 x_i}{d|x_i - b_1|} \\ &+ \left(sin^{-1}\frac{b_2}{d} - sin^{-1}\frac{b_1}{d}\right)\sqrt{d^2 - x_i^2}\Bigg] F(b_1, b_2, d) \end{aligned} \tag{2.12}$$

$$F(b_1, b_2, d) = \left[\frac{sin^{-1}\left(\dfrac{sin\frac{\pi b_2}{2b}}{sin\frac{\pi d}{2b}}\right) - sin^{-1}\left(\dfrac{sin\frac{\pi b_1}{2b}}{sin\frac{\pi d}{2b}}\right)}{sin^{-1}\frac{b_2}{d} - sin^{-1}\frac{b_1}{d}}\right]\sqrt{sec\frac{\pi d}{2b}} \tag{2.13}$$

where $b_2 = x_j + w_j$, $b_1 = x_j - w_j$, w_j is the width of strip j and

$$E' = \begin{cases} E & \text{for plane stress} \\ \frac{E}{1-\upsilon^2} & \text{for plain strain} \end{cases}$$

where E is the elastic modulus and υ is Poisson's ratio.

2.2.3. FATIGUE CRACK GROWTH MODEL

In the present model, fatigue crack growth is predicted using the Paris law:

$$\frac{da}{dN} = C_1 \Delta K^{n\prime} \tag{2.14}$$

ΔK is expressed in terms of a dimensionless constant, *F*, which is a function of the specimen geometry:

$$\Delta K = F \Delta\sigma \sqrt{\pi a} \tag{2.15}$$

Equations (2.4) and (2.5) can be integrated analytically using separation of variables:

$$\frac{da}{a^{n/2}} = C_1 \left(F \Delta\sigma \sqrt{\pi}\right)^{n\prime} dN \tag{2.16}$$

$$\int_{a_i}^{a_{i+1}} \frac{da}{a^{n/2}} = \int_{N_i}^{N_{i+1}} C_1 \left(F \Delta\sigma \sqrt{\pi}\right)^{n\prime} dN \tag{2.17}$$

Integrating both sides of Equation (2.8), rearranging and solving for the final crack length, gives the following:

$$a_{i+1}^{\frac{2-n'}{2}} = a_i^{\frac{2-n'}{2}} \left(1 - \frac{n'-2}{2a_i} C_1 \left(F\Delta\sigma\sqrt{\pi a}\right)^{n'} \Delta N\right) \tag{2.18}$$

$$a_{i+1} = a_i \left(1 - \frac{n'-2}{2a_i} C_1 \left(F\Delta\sigma\sqrt{\pi a}\right)^{n'} \Delta N\right)^{\frac{2}{2-n'}} \tag{2.19}$$

Equation (2.10) can be generalized for a crack characterized by the Paris law in an arbitrary geometry as follows:

$$a_{i+1} = a_i \left(1 - \frac{n'-2}{2a_i} \left(\frac{da}{dN}\right) \Delta N\right)^{\frac{2}{2-n'}} \tag{2.20}$$

Using Equation (2.11), the amount of crack extension due to fatigue crack growth can be directly calculated for each time interval. Since the focus of the present model is the interaction of creep and fatigue crack growth, Equation (2.11) will be used to calculate the contribution of fatigue crack growth to total crack extension over a time interval.

2.2.4. Implementation of the Empirical Creep Model

In the strip yield model, the displacement, V_j, is measured from the crack centerline (see Figure 2.2).

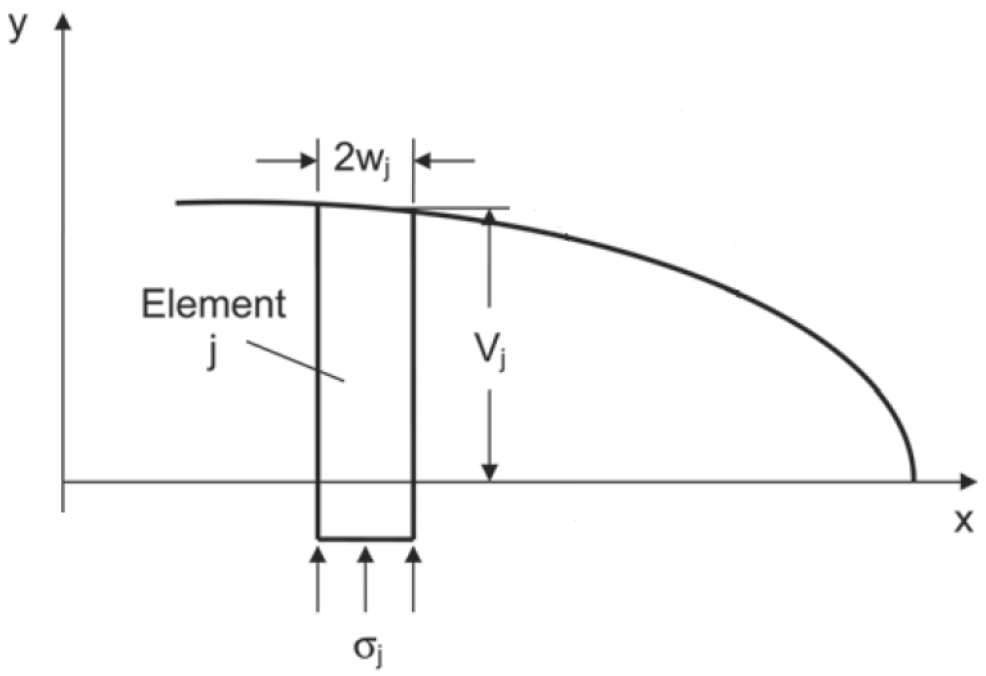

Fig. 2.2 – Schematic of yield strip displacement and width

If V_n is the displacement of the strip at the crack tip, the crack tip opening displacement (CTOD), ϕ, is:

$$\phi = 2V_n \tag{2.21}$$

where V_n is the displacement of the strip at the crack tip.

For the elements in the process zone, the creep deformation is modeled by the secondary creep strain rate, $\dot{\varepsilon}_s$, defined by the Norton power law:

$$\dot{\varepsilon}_s = A\left(\frac{\sigma}{G}\right)^n \tag{2.22}$$

where A, n are constants specific to a material and temperature, G is the shear modulus of the material and σ is the applied stress.

Applying Equation (2.22) to the strip-yield model, the rate of change of the CTOD due to secondary creep strain is:

$$\dot{\phi} = \lambda A \left(\frac{\sigma_0}{G}\right)^n \tag{2.23}$$

where σ_0 is the applied stress in the creep process zone (the flow stress) and λ is a material characteristic length [3]

The evolution of creep damage in the creep process zone is then simulated by calculating the CTOD and adjusting the flow stress based on this calculation, i.e., for time increment *k+1*:

$$\phi_{k+1} = \phi_k + \dot{\phi}_k \Delta t \tag{2.24}$$

$$\sigma_{0k+1} = \frac{\sigma f(x_i) - \phi_{k+1}}{\sum_{j=1}^{n} g(a, x_j)} \tag{2.25}$$

Tertiary creep crack extension begins when the CTOD reaches a critical value, which is determined experimentally. The creep crack extension used here was proposed by Nikbin, Smith and Webster (for whom it was named the NSW model) and discussed by Webster and Ainsworth [6, 7] and correlates the creep crack extension rate, $\dot{a}$, to the *C** contour integral:

$$\left(\frac{da}{dt}\right)_{time} = \dot{a} = \frac{(n+1)A}{\varepsilon_f^*}\left(\frac{C^*}{I_N G A}\right)^{n/(n+1)} r_c^{1/(n+1)} \tag{2.26}$$

where *A* is the coefficient from the secondary creep power law, *n* is the exponent from the secondary creep power law, *G* is the shear modulus of the material, r_c is the radius of the creep process zone (assumed to be equal to ρ, the creep process zone size calculated with the strip-yield

model above) and ε_f^* is the creep ductility. $\varepsilon_f^* = \varepsilon_f$ for plane stress constraint, $\varepsilon_f^* = \varepsilon_f/50$ for plane strain constraint and ε_f is the uniaxial creep failure strain [6].

$I_{N\prime}$ is a non-dimensional function of the plastic strain hardening exponent N'. $I_{N\prime}$ was determined numerically in [8] to be:

$$I_{N\prime} = 7.2\left(0.12 + \frac{1}{N\prime}\right)^{1/2} - \frac{2.9}{N\prime} \text{ for plane stress.} \tag{2.27a}$$

$$I_{N\prime} = 10.3\left(0.13 + \frac{1}{N\prime}\right)^{1/2} - \frac{4.6}{N\prime} \text{ for plane strain.} \tag{2.27b}$$

Webster and Ainsworth [6] note that for most materials, the secondary creep exponent n is a good approximation for the strain hardening exponent N'.

Since *C** is the only term in Equation (2.26) that varies with time, the creep crack extension rate equation can be simplified to:

$$\dot{a} = D_0 C^{*\phi} \tag{2.28}$$

where:

$$D_0 = \frac{(n+1)A}{\varepsilon_f^*}\left(\frac{1}{I_n GA}\right)^{n/(n+1)} \rho^{1/(n+1)} \tag{2.29}$$

$$\phi = \frac{n}{(n+1)} \tag{2.30}$$

For linear elastic problems, the *C** integral can be approximated as [6]:

$$C^* = \frac{P\dot{\Delta}^c}{B(w-a)}\frac{n}{(n+1)}\eta_p \tag{2.31}$$

where P is the applied load, B is the out of plane thickness of the specimen, w is width (half width for center-cracked tension specimens), n is the creep strain rate exponent, η_p is a non-dimensional function of the specimen geometry (tabulated values are provided in [6]) and $\dot{\Delta}^c$ is the load line displacement rate due to creep. In order for this approximation to be valid the overall response must be linear elastic, i.e., the size of the plastic zone (creep process zone) must be sufficiently small compared to the size of the specimen so that the specimen can be considered essentially infinite (an order of magnitude difference in these dimensions is commonly used as a practical criteria).

$\dot{\Delta}^c$ can be approximated from handbook solutions for the J-integral functions h_1 and h_3, or by explicitly differentiating Δ^c from elastic handbook solutions. The present model will approximate $\dot{\Delta}^c$ by the following relationship:

$$\dot{\Delta}^c \approx \dot{\varepsilon}_s = A\left(\frac{\sigma}{G}\right)^n \tag{2.32}$$

2.2.5. Implementation of the Constitutive Creep Model

An alternative approach to the Norton power law for creep deformation is to use a microstructure-based constitutive model for creep that takes into account the generation, glide, climb and annihilation of dislocations. In the present model, a constitutive model for the creep deformation and damage that was developed by Basirat et al. [9] will be used. In order to adapt Basirat et al. model to the strip yield methodology, recall Orowan's equation for creep deformation resulting from dislocation mobility:

$$\dot{\varepsilon} = \frac{\rho_m b v_g}{M} \tag{2.33}$$

where b is the Burger's vector, M is the Taylor factor, v_g is the dislocation glide velocity and ρ_m is the density of the mobile dislocations.

Orowan's equation was modified [9] to include three damage terms:

$$\dot{\varepsilon} = \frac{\rho_m b v_g}{M(1-D_s)(1-D_p)(1-D_N)} \tag{2.34}$$

where D_s is the damage caused by depletion of the solid solution of the Fe_2Mo laves phase, D_p is the damage due to precipitate particle ($M_{23}C_6$) coarsening and D_N is the damage due to void nucleation and crack formation.

These damage terms will be discussed in further detail below. A system of equations was developed that defines relationships for the terms in the modified Orowan's equation (Equation (2.34)). The density of mobile dislocations was defined using the equations

$$\rho = \rho_m + \rho_{dip} \tag{2.35}$$

$$\dot{\rho}_m = \dot{\rho}_{m,gen} - \dot{\rho}_{m,spon} - \dot{\rho}_{dip,gen} \tag{2.36}$$

$$\dot{\rho}_{dip} = \dot{\rho}_{dip,gen} - \dot{\rho}_{dip,spon} - \dot{\rho}_{dip,c} \tag{2.37}$$

$$\dot{\rho}_{m,gen} = \frac{M\dot{\varepsilon}}{b\Lambda} \tag{2.38}$$

The density rates in Equations (2.35)-(2.38) are the rates of generation, spontaneous annihilation and climb annihilation of mobile dislocations (subscript m) and dislocation dipoles (subscript dip). The term Λ in Equation (2.38) is defined as follows:

$$\Lambda = \frac{k_\Lambda}{\sqrt{\rho}} \tag{2.39}$$

where k_A is a function of stress and temperature (determined experimentally).

The rate of mobile dislocation annihilation is:

$$\dot{\rho}_{m,ani} = \frac{4M\dot{\varepsilon}d_{dip}\rho_m}{b(n_g)} \tag{2.40}$$

where n_g is the number of active slip planes and d_{dip} is defined as:

$$d_{dip} = \frac{M}{8\pi(1-\upsilon)}\frac{Gb}{\sigma} \tag{2.41}$$

where G is the shear modulus and σ is the applied stress.

The rate of spontaneous and climb annihilation of mobile dislocations ($\dot{\rho}_{m,spon}$ and $\dot{\rho}_{dip,c}$) is:

$$\dot{\rho}_{m,spon} = \frac{d_{spon}}{d_{dip}}\dot{\rho}_{m,ani} \tag{2.42}$$

$$\dot{\rho}_{dip,c} = \rho_{dip}\frac{4v_c}{(d_{dip}-d_{spon})} \tag{2.43}$$

d_{spon} represents the separation distance between two mobile dislocations at which the dislocations will spontaneously form a dipole. d_{spon} is obtained by solving the following:

$$v_c = \frac{D\Omega\sigma_c}{bK_BT} \tag{2.44}$$

$$\sigma_c + \frac{v_c}{B} = \frac{Gb}{2\pi(1-\upsilon)}\frac{2}{(d_{spon}+d_{dip})} \tag{2.45}$$

$$B = \frac{9\Omega D_{sol} K_B T}{M C_0 G^2 b^7 \varepsilon_a^2 \, ln\left(\frac{r_2}{r_1}\right)} \tag{2.46}$$

where v_c is the dislocation climb velocity, Ω is the atomic volume, σ_c is the climb stress, K_B is the Boltzmann constant, T is the temperature, B is the dislocation mobility term, D_{sol} is the coefficient of self-diffusion, C_0 is the solute concentration, ε_a is the relative size misfit between solute and solvent atoms and r_2 and r_1 are the outer and inner cut-off radii of the dislocation stress field.

The spontaneous rate of annihilation of dipoles is an athermal process, and can be expressed:

$$\dot{\rho}_{dip,ani} = \frac{2M\dot{\varepsilon}d_{spon}\rho_{dip}}{b(n_g)} \tag{2.47}$$

The dislocation glide velocity is formulated [9] as follows:

$$\sigma^* = \sigma - \sigma_i \tag{2.48}$$

$$\sigma_i = \alpha MCGb\sqrt{\rho_m + c_{dip}\rho_{dip}} \tag{2.49}$$

$$v_g = B\sigma^* \tag{2.50}$$

where σ^* is the effective stress, σ_i is the athermal stress component resulting from the inter-dislocation interaction, α is a dislocation interaction constant, C is the inelastic deformation factor and c_{dip} is a weight factor.

Orowan's equation was modified to include three damage terms developed for modified 9Cr-1Mo steel, as mentioned above. These damage terms must be solved implicitly in the present constitutive model along with the creep strain rate. The damage terms are defined as follows:

Damage due to solid solution depletion:

$$D_s = 1 - \frac{\bar{C}_t}{C_0} \tag{2.51}$$

$$\dot{D}_s = K_s D_s^{1/3}(1 - D_s) \tag{2.52}$$

$$K_s = \left[48\pi^2 \left(c_0 - \frac{c_e}{c_\beta}\right)^{1/3} n^{2/3} D\right] \tag{2.53}$$

where C_0 is the initial concentration of solid solution, $\bar{C}_t$ is the concentration at time *t*, c_0, c_e are calculated values, c_β is the concentration of solid solution in the precipitate of laves, *n* is the number of precipitate particles, *D* is the diffusion coefficient of Mo in matrix.

Damage due to precipitate particle coarsening:

$$D_p = 1 - \frac{P_0}{P_t} \tag{2.54}$$

$$\dot{D}_p = \frac{k_p}{3}\left(1 - D_p\right)^4 \tag{2.55}$$

where P_0 is the initial particle diameter, P_t is the particle size at time *t*.

Damage due to void nucleation and crack formation:

$$D_N = A\dot{\varepsilon}\varepsilon^{0.9} \tag{2.56}$$

where *A* is an empirical fitting constant.

These equations describe the physics of creep deformation in terms of dislocation mobility (glide and climb) and continuum damage. The present model will solve the modified Orowan equation using Runge-Kutta implicit integration for the creep strain rate ($\dot{\varepsilon}$).

The constitutive method uses the strip yield model to apply the creep constitutive equation for uniaxial strain (Orowan's equation) to creep crack growth. Each crack tip element is analyzed as loaded under a uniaxial creep strain state. As the life progresses, crack tip strips accumulate creep strain until the creep ductility is reached. At this point, the strip is considered to have failed. The crack length is advanced by the width of the yield strip and the analysis continues.

2.2.6. Model Interaction

The present model was implemented in a computer program to enable effective comparison of the model predictions to test data. The computer program allows the desired creep model to be selected and fatigue loading to be turned on or off. Regardless of the creep model used, the problem being studied is divided into a specified number of time intervals and final results are solved explicitly in time. For each time increment, the amount of creep crack growth and fatigue crack growth are calculated. The crack length is extended by the sum of these values and the position of the yield strips in the creep process zone is updated accordingly. This process is repeated until the requested life time has been analyzed or the limit load is reached in the remaining ligament.

This implementation assumes that the stress in the creep process zone is constant, the crack tip constraint is approximately plane stress and that the specimen of interest can be reasonably approximated by a thin, center-cracked plate.

Studies of the NSW model may additionally need to consider the effects of initiation time. Crack initiation requires the specification of a criterion for the onset of crack growth; either a critical CTOD or a predetermined time period. Prior to initiation there is no creep crack growth. After initiation, creep crack growth is handled in the same way as fatigue crack growth: an increment of crack length is calculated, added to the current crack length and the positions of the yield strips are updated.

Studies of the constitutive creep model do not need to consider initiation time as this is part of the constitutive model. An increment of creep crack growth is considered to occur when the accumulated strain at a yield strip reaches the creep ductility. During each time increment, the computer program updates the creep strain at each yield strip. If a yield strip reaches the creep ductility in a time increment, the crack length is increased by the width of the failed yield strip. The strip is removed and additional undamaged strips are added to the end away from the crack tip to maintain the size of the creep process zone computed according to Equation (2.15).

2.3. RESULTS

2.3.1. EXPERIMENTAL DATA

The present models were compared to experimental data available in the literature. Creep-fatigue and pure fatigue tests were performed on Compact Tension (C(T)) specimens at 625ºC [1]. Pure creep tests were conducted on C(T) specimens at 650ºC [10]. Barker et. al. [11] conducted a series of creep crack extension tests at 525ºC on double edge notched tension (DEN(T)) specimens. Substantial hardening due to plastic deformation was reported in the high stress specimens and much less in the low stress specimens. Each experiment was modeled using both the NSW model and the constitutive model, so that the results can be compared.

Material properties used for the NSW model are provided in Table 2.1, and material properties used for the constitutive creep model are presented in Table 2.2. Material properties are assumed to be the same for both sets of data since the experimental conditions are consistent.

Table 2.1 – Material Properties, NSW Model.

Property (unit)	**Value [Reference]**
σ_0 (MPa)	334.4 [1]
E (MPa)	1.25E+05 [1]
υ (-)	0.3
A (-)	1.75E+20 [10]
n (-)	8.462 [10]
ε_f^* (mm/mm)	0.18 [11]

Table 2.2 – Material Properties, Constitutive Model.

Property (unit)	**Value [Reference]**
σ_0 (MPa)	334.4 [1]
E (MPa)	1.25E+05 [1]
υ (-)	0.3
ε_f^* (mm/mm)	0.18 [11]
b (μm)	2.47E-04 [9]
M (-)	3 [9]
ρ_m (m^{-2})	1.2E+14 [9]

Values of other constants in the model discussed in Section 2.2.5 were taken from reference [9]. Fatigue crack growth constants used for creep-fatigue and pure fatigue experiments are presented in Table 2.3. Specimen geometry and loading for the experiments in each reference are summarized in Table 2.4. Specimen thickness documented in Table 2.4 is the effective thickness of the specimen for side-grooved specimens [10] (marked with *).

Table 2.3 – Fatigue Crack Growth Constants.

Property (unit)	**Value [Reference]**
C_1 (mm/cycle)	1.75E+20 [6]
n (-)	8.462 [6]
ΔK_{th} (MPa $\sqrt{\mathrm{m}}$)	5 [6]

Since all of these specimens were pre-cracked, creep crack growth is assumed to begin at the commencement of the experiment (i.e., crack initiation time assumed to be zero). Specimens 3-1-1W, 3-1-8B and 3-1-9B were subjected to pure fatigue loading [1]. Specimens 3-1-2W and 3-1-4W were subjected to creep-fatigue loading with a tensile hold of 60 seconds at the peak of each cycle. Specimens 3-1-3W and 3-1-5W were subjected to creep-fatigue loading with a tensile hold of 600 seconds at the peak of each cycle.

Table 2.4 – Experimental Specimen Geometry.

Experiment	**Initial crack size (mm)**	**Width (mm)**	**Thickness (mm)**	**Applied stress (MPa)**	**Cyclic load ratio (-)**
3-1-1W [1]	20.25	50.0	12.5	49.2	0.1
3-1-8B [1]	19.54	50.0	12.5	50.2	0.1
3-1-9B [1]	20.17	50.0	12.5	60.4	0.1
3-1-2W [1]	19.90	50.0	12.5	50.0	0.1
3-1-3W [1]	20.27	50.0	12.5	49.2	0.1
3-1-4W [1]	19.92	50.0	12.5	41.5	0.1
3-1-5W [1]	19.95	50.0	12.5	41.5	0.1
CT1* [10]	15.50	32.0	8.0	54.2	N/A
CT2* [10]	15.50	32.0	7.6	45.7	N/A
CT3* [10]	15.50	32.0	7.2	43.4	N/A
CT4* [10]	15.50	32.0	7.2	36.2	N/A
DENT1 [11]	2.475	15.0	6.0	202.	N/A
DENT2 [11]	2.475	15.0	6.0	215.	N/A
DENT3 [11]	2.475	15.0	6.0	225.	N/A
DENT4 [11]	2.475	15.0	6.0	250.	N/A

2.3.2. Comparison to Model Predictions

Figures 2.3-2.5 compare the final crack length predicted by the constitutive and NSW models to the experimental data [1]. Note that the pure fatigue experimental results are shown with the constitutive model only because the pure fatigue results employ no creep model.

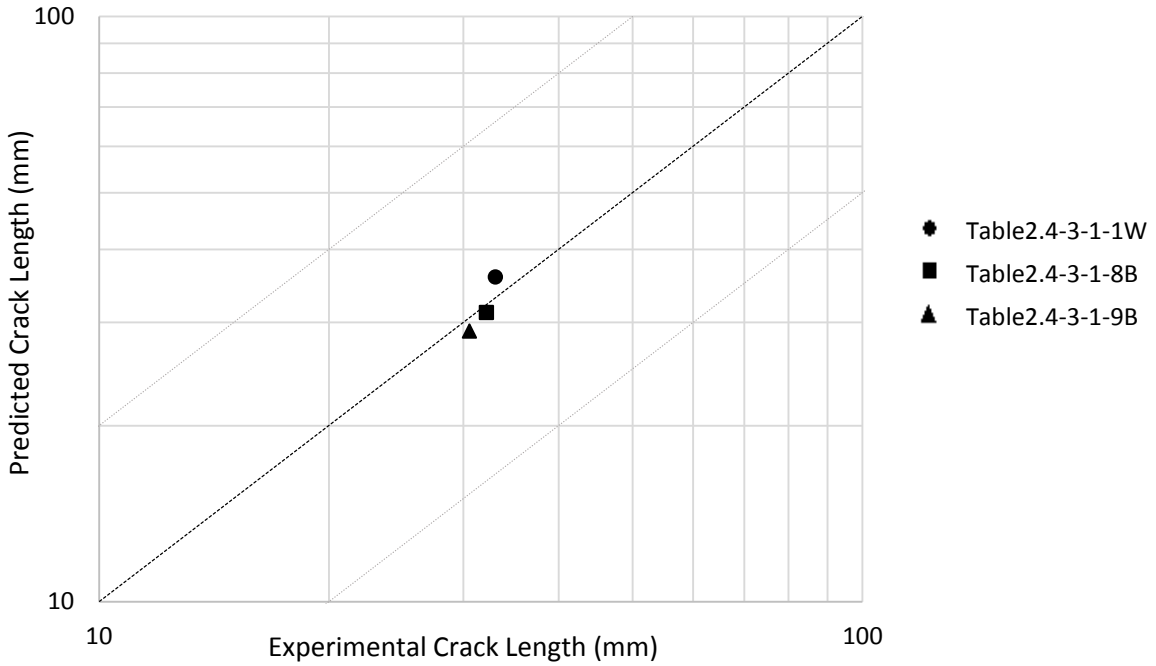

Fig. 2.3 – Predicted versus experimental final crack length for fatigue crack growth.

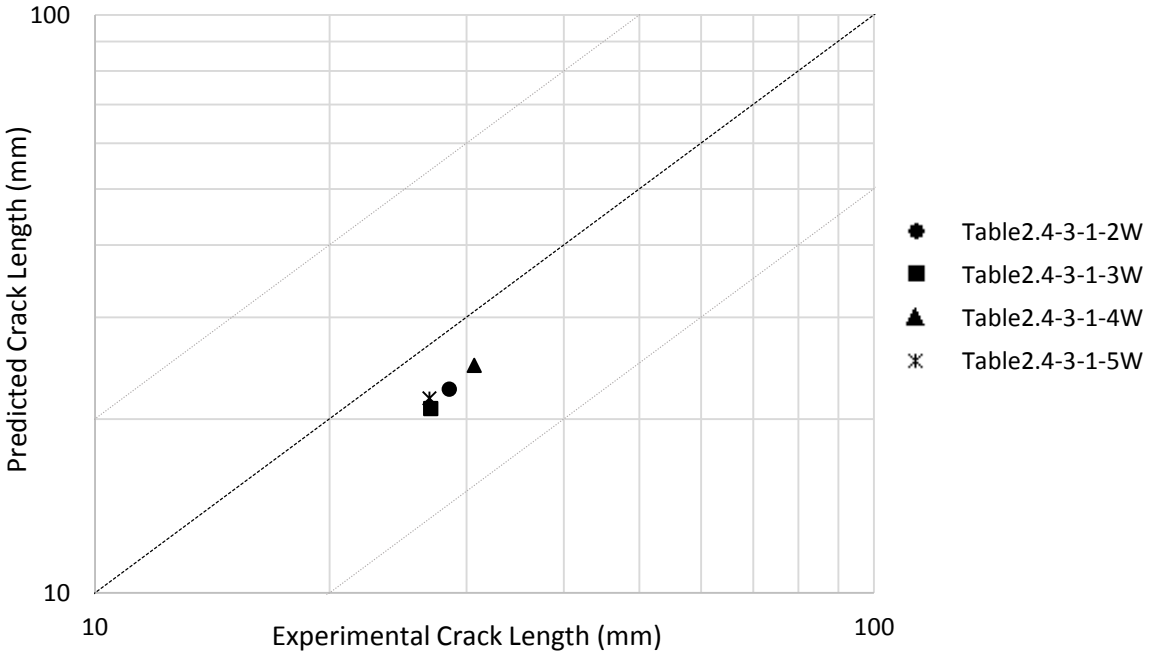

Fig. 2.4 – Predicted versus experimental final crack length using the constitutive creep model and fatigue crack growth.

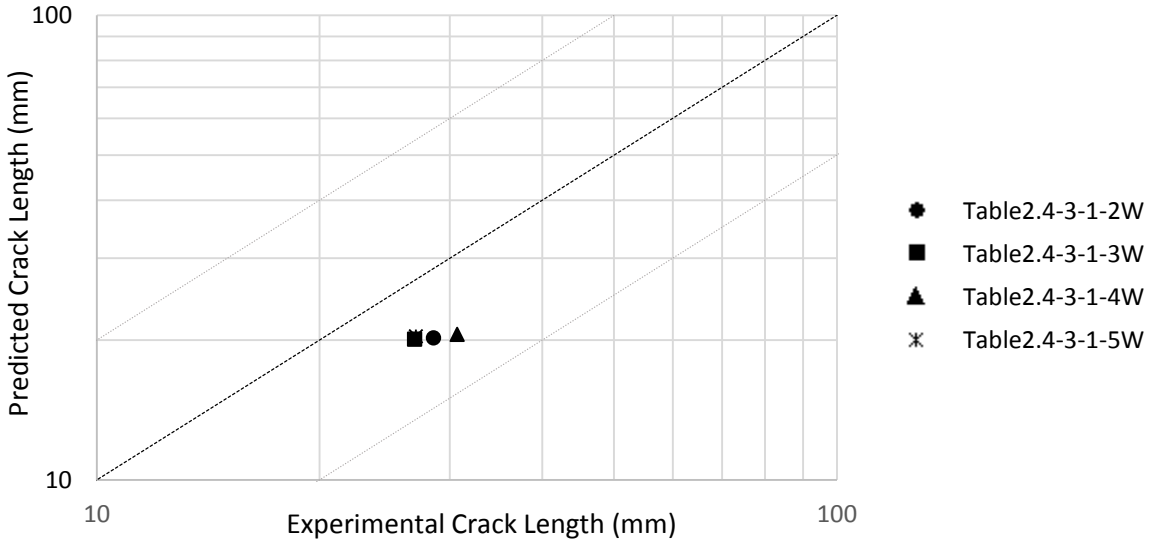

Fig. 2.5 – Predicted versus experimental final crack length using the empirical model.

Figure 2.6 compares the results of the constitutive model to the data from [10]. No results are presented for the NSW model, because this model predicted that over 100,000 hours would be insufficient to cause failure in these specimens. This is such a significant deviation from the experimental results that plotting such data becomes both impractical and meaningless.

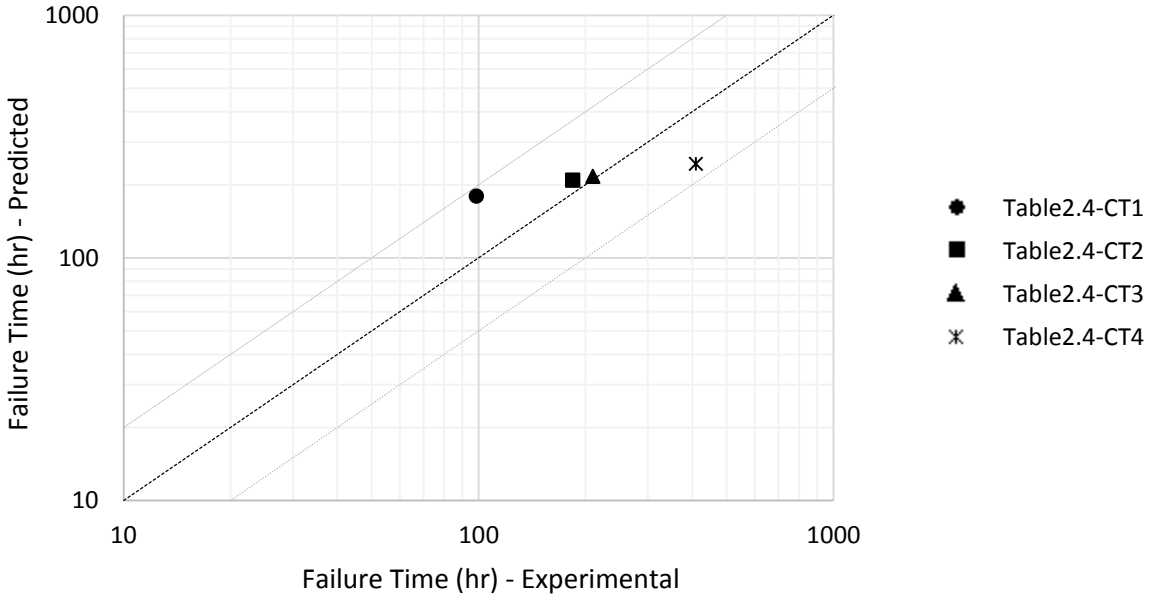

Fig. 2.6 – Predicted versus experimental failure time using the constitutive creep model.

Figure 2.7 shows the results of the empirical model compared to the experimental data and Figure 2.8 shows the results of the constitutive model compared to the experimental data [11].

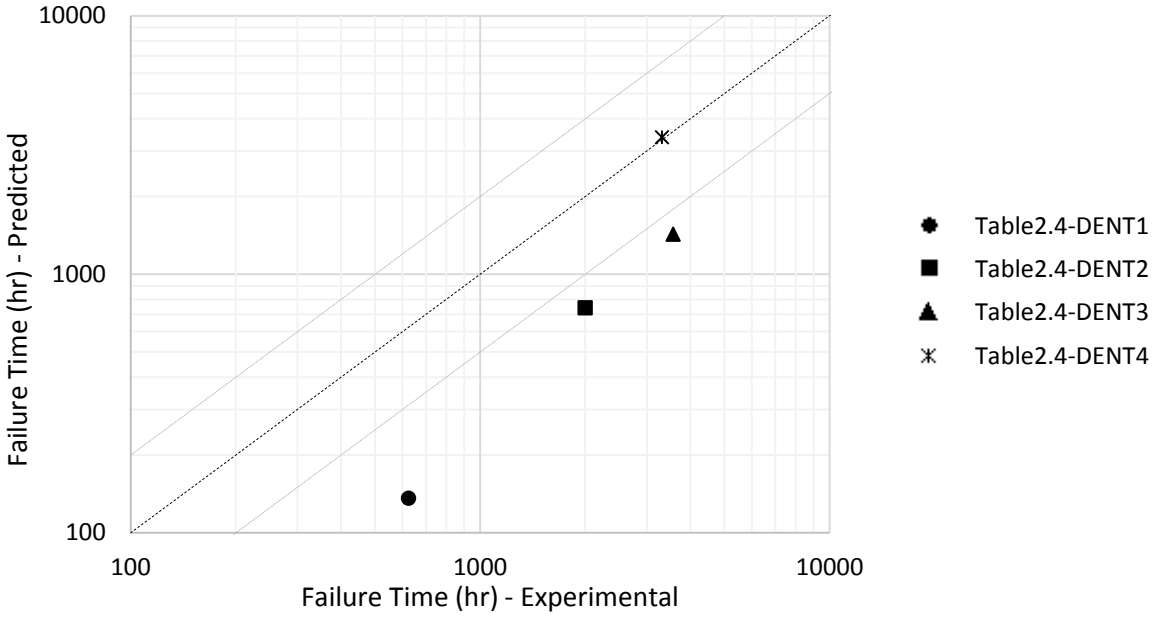

Fig. 2.7 – Predicted versus experimental failure time using the empirical model.

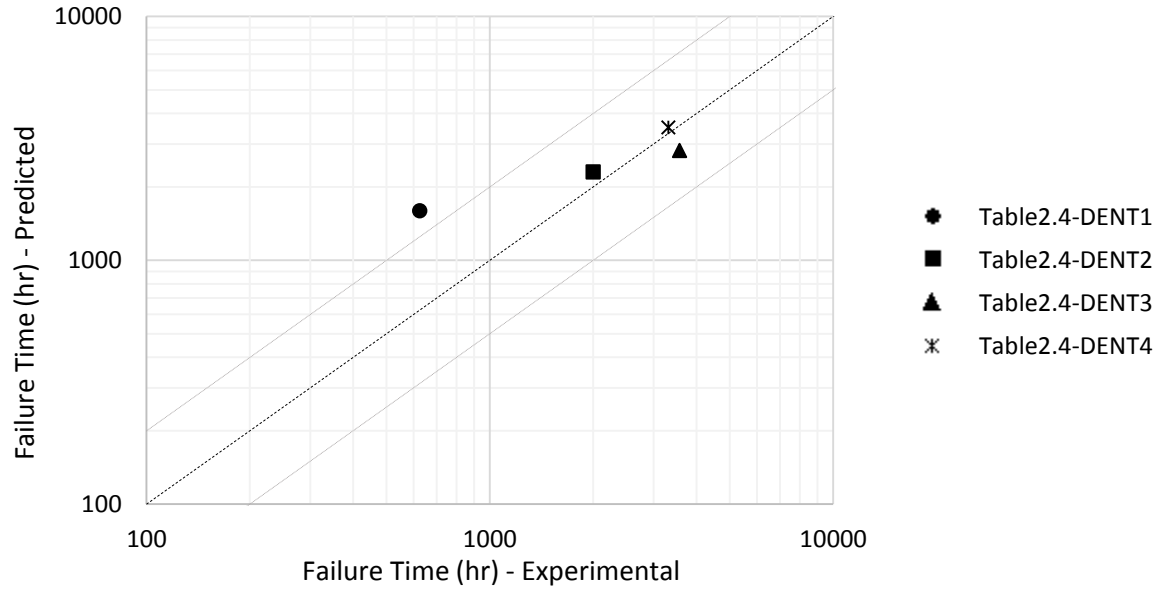

Fig. 2.8 – Predicted versus experimental failure time using the constitutive model.

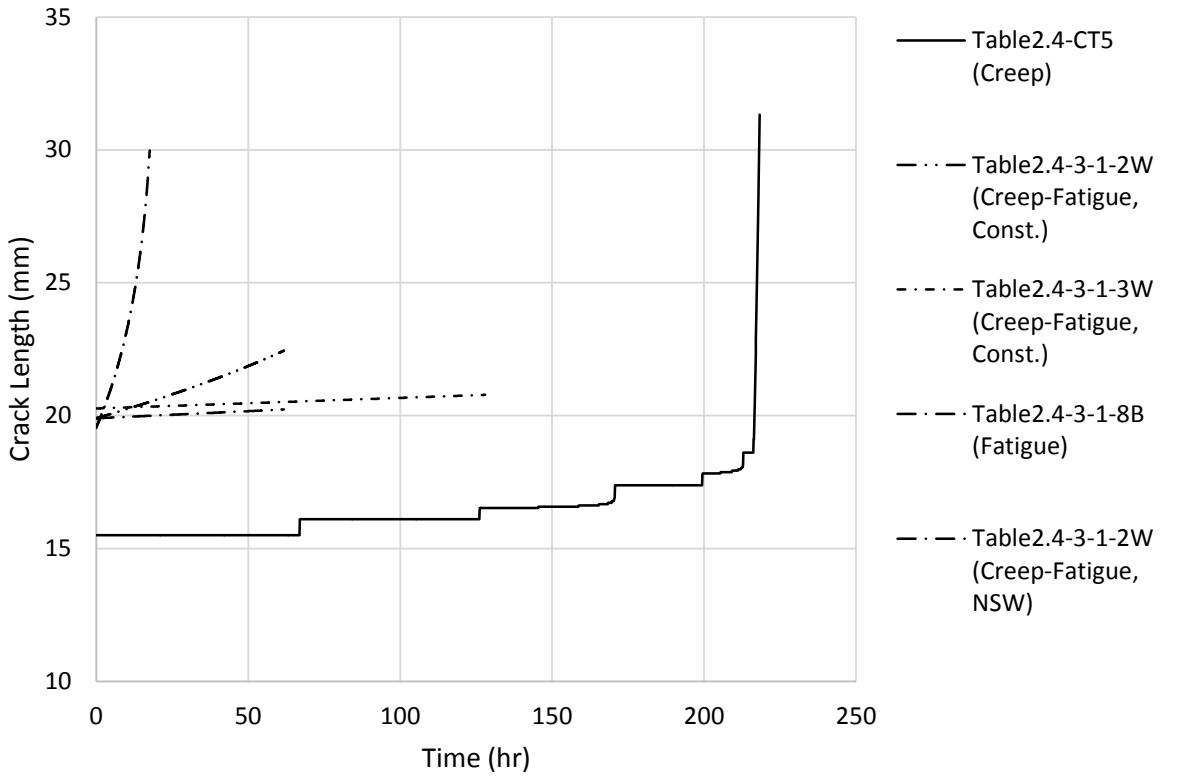

Fig. 2.9 – Predicted crack length versus time in specimens experiencing pure creep, creep-fatigue and pure fatigue.

Figure 2.9 shows crack length over time for several representative specimens. Note the discontinuities in the pure creep data, caused by several yield strips failing simultaneously. This is expected since the strip yield model assumes that the creep process zone experiences a constant load: the flow stress. The same behavior is avoided for creep-fatigue analyses because the crack is also growing due to fatigue. These interactions will be discussed in detail in Chapter 4.

Figures 2.10-2.11 compare the crack extension rates between two creep-fatigue tests, one with a 600 second hold time (Figure 2.10) and one with a 60 second hold time (Figure 2.11).

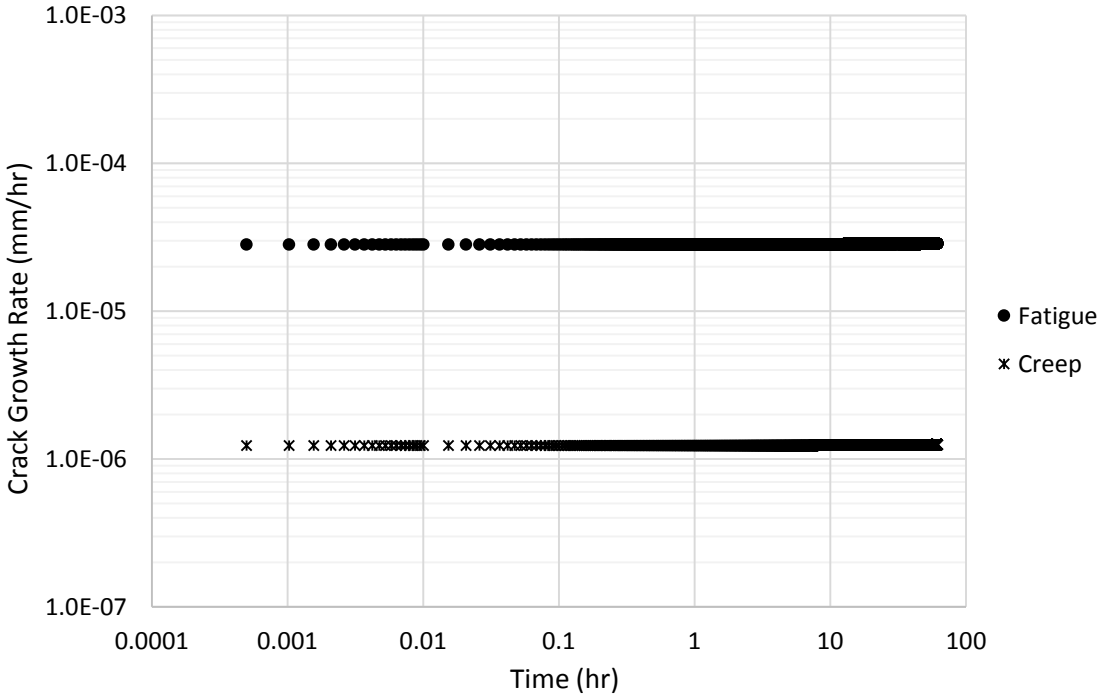

Fig. 2.10 – Predicted crack growth rate in fatigue and creep versus time in specimen 3-1-2W.

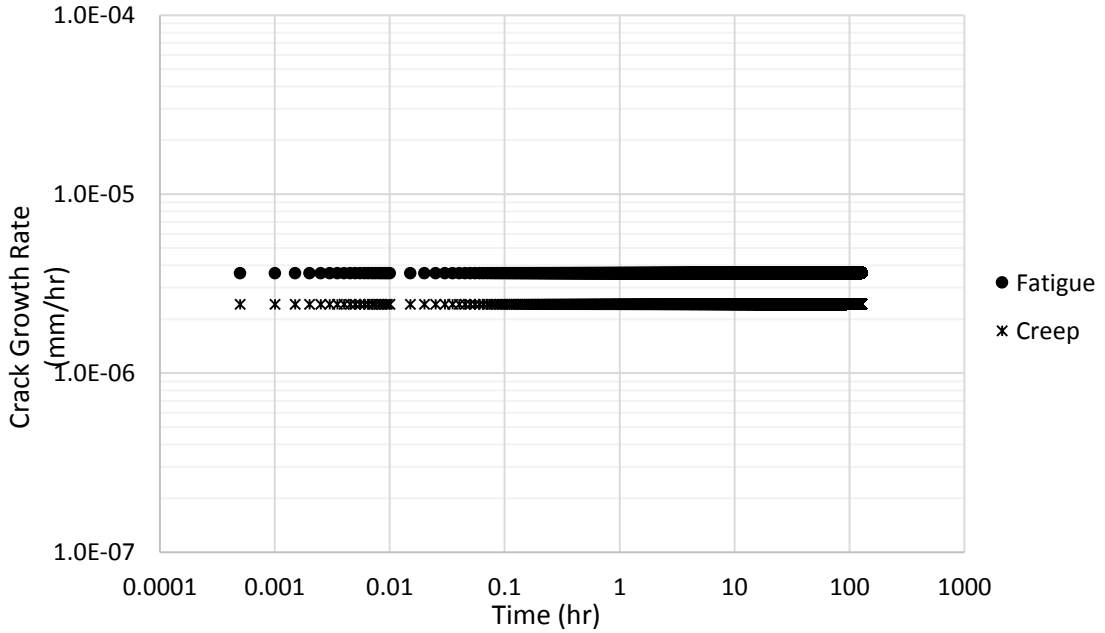

Fig. 2.11 – Predicted crack growth rate in fatigue and creep versus time in specimen 3-1-3W.

The NSW model studied assumes the stress-strain field is of the non-linear elastic type described by Hutchinson, Rice and Rosengren (HRR type). In the experimental data examined in the present study, the applied stresses were low (approximately 15% of the yield stress). As a result, the calculated size of the creep process zone was small compared to the other dimensions of the specimen. In this situation, the behavior is dominated by the linear elastic response, rather than the non-linear response. Since this is the case, a linear elastic crack tip parameter such as the stress intensity factor would be expected to correlate well to the experimental data. The C^* contour integral approximation may not correlate as well to creep crack growth under these conditions (Figures 2.3 and 2.4 show the NSW model significantly under predicts the crack growth relative to these experiments). The results shown in Figures 2.6-2.8 suggest some of the assumptions behind the model may not apply to experimental conditions represented. Model assumptions will be verified and discussed in Chapter 4.

The constitutive model also under predicts the majority of the experimental data (the notable exceptions being some of the pure creep experiments), however, it agreed more closely with the test data than the NSW model. The constitutive model requires several constants to be fitted to uniaxial test data to obtain accurate results. The present study used the fitting constants available in the literature [9], which cover a stress range of 80-200 MPa. The stresses in the present study are outside of this stress range, which is expected to be a contributing factor to the under prediction of test data.

There is uncertainty in the experimental data that must also be considered. Although neither [1] nor [10] attempted to quantify the experimental uncertainty, [13] showed that for similar experiments the uncertainty could be around 40%. This indicates that constitutive model is within the scatter in the experimental data, which is in agreement with the conclusion that the model may require only slight adjustment (such as development of fitting constants in the appropriate stress range).

2.4. CONCLUSIONS

The present model for creep crack growth was developed based on the creep constitutive equation proposed in [9]. This equation was shown in [9] to be effective at predicting creep in uniaxial test specimens. A strip yield model is used to represent the creep process zone as a series of yield strips [4]. The constitutive model in [9] is applied to each yield strip and the constitutive equations are implicitly solved for the creep strain at each time increment. In order to study the interaction of creep and fatigue crack growth, the effects of cyclic loading were implemented in the present model using the Paris Law.

The NSW model was also implemented with the Paris Law. The NSW model empirically correlates creep crack extension with C^*, a contour integral analogous to J-integral. C^* is a valid crack tip parameter only for HRR type stress-strain fields [14]. The NSW model explicitly predicts the creep crack growth at each time increment.

These models were compared to test data presented in [1] and [10] with mixed results. The NSW model did not predict the [1] and [10] experimental data well. The applied stresses in these tests were low (approximately 15% of the yield stress). Therefore the behavior is dominated by the linear elastic response, rather than the visco-plastic response. Since this is the case, the C^* contour integral may not correlate well to creep crack growth. It has shown good agreement to experimental data in the literature for higher stress tests [6, 15, 16].

The constitutive model agreed more closely with the test data, though it still under predicted the majority of the data. This model requires several fitting constants to uniaxial test data to obtain accurate results. The present study used the fitting constants available in [9]; however, the stresses in the present study are outside of the stress range for these constants. This is expected to be a contributing factor to the under prediction of test data. Uncertainty in the test data is also a possible contributing factor.

Studies presented in Chapter 3 will expand on the findings in this chapter by expanding the constitutive model to AISI 316L stainless steel and comparing model predictions to additional sets of data.

2.5. REFERENCES

[1] Narasimhachary SB, Saxena A. Crack growth behavior of 9Cr-1Mo (P91) steel under creep–fatigue conditions. International J. of Fatigue. 2013;56:106–13.

[2] Liu H, Bao R, Zhang J, Fei B. A creep–fatigue crack growth model containing temperature and interactive effects. International J. of Fatigue. 2014;59:34–42.

[3] Potirniche GP. A Numerical Strip-Yield Model for the Creep Crack Incubation in Steels. J. of ASTM International. 2012;9(3):1-13.

[4] Dugdale DS. Yielding of Steel Sheets Containing Slits. J. Mechanics & Phys. of Solids. 1960;8:100–4.

[5] Tada H, Paris PC, Irwin GR. The Stress Analysis of Cracks Handbook. Third ed. New York (NY): American Society of Mechanical Engineers; 2000.

[6] Webster GA, Ainsworth RA. High Temperature Component Life Assessment. First ed. London: Chapman & Hall; 1994.

[7] Nikbin KM, Smith DJ, Webster GA. An engineering approach to the prediction of creep crack growth. J. Engineering Material Technology. 1986;108:186–91.

[8] Anderson TL. Fracture Mechanics: Fundamentals and Applications. Third ed. Boca Raton (FL): CRC Press; 2005.

[9] Basirat M, Shrestha T, Potirniche GP, Charit I, Rink K. A study of the creep behavior of modified 9Cr–1Mo steel using continuum-damage modeling. International J. of Plasticity. 2012;37:95–107.

[10] Hyde TH., Saber M, Sun W. Creep crack growth data and prediction for a P91 weld at 650ºC. International J. of Pressure Vessels and Piping. 2010;87: 721-29.

[11] Barker E, Lloyd GJ, Pilkington R. Creep Fracture of a 9Cr-lMo Steel. Materials Science and Engineering. 1986;84:49-64.

[12] Maleki S, Zhang Y, Nikbin K. Prediction of creep crack growth properties of P91 parent and welded steel using remaining failure strain criteria. Engineering Fracture Mechanics 2010;77:3035-42.

[13] Vainshtok VA, Baumshtein MV, Makovetskaya IA, Kramarenko IV. Creep Crack Growth Laws in Heat Resistant Steels. Engineering Fracture Mechanics. 1991;40(6):1147-63.

[14] Rice JR. Mathematical analysis in the mechanics of fracture. In: Liebowitz, H, editor. Treatise on fracture. Vol. 2, New York, NY: Academic Press; 1968.

[15] Brust FW, Majumdar BS. Load History Effects on Creep Crack Growth. Engineering Fracture Mechanics, 1994;49(6):809-37.

[16] Saxena A. Creep Crack Growth in High Temperature Ductile Materials. Engineering Fracture Mechanics. 1991;40(4/5):721-36.

Chapter 3 – Application of Implicit Creep-Fatigue Lifetime Assessment Method to AISI 316L Stainless Steel

3.1. INTRODUCTION

As previously recommended in Chapter 2, expansion of the constitutive model would be helpful in showing the practicality of the proposed model as well as better identifying and quantifying the limitations of the model. This study will extend the constitutive model to AISI 316L stainless steel, a corrosion resistant steel often found in high temperature applications, and compare analytical to experimental results for 316L stainless steel.

3.2. THEORY & METHODS

3.2.1. CALCULATION OF 316L STAINLESS STEEL MATERIAL CONSTANTS

In order to extend the constitutive creep model presented in Chapter 2 to 316L stainless steel, microstructural material properties and empirical constants must be obtained for the terms in the governing equation (Equation (2.34)):

$$\dot{\varepsilon} = \frac{\rho_m b v_g}{M(1-D_s)\left(1-D_p\right)(1-D_N)} \tag{3.1}$$

The terms D_s and D_p in Equation 3.1 are specific to microstructural material properties of modified 9Cr-1Mo steel and cannot necessarily be applied to another material. Since developing creep damage terms related to the microstructural material properties of 316L stainless steel is beyond the scope of this study, the 316L creep model will be based on the unmodified form of Orowan's equation. Orowan's equation does not account for tertiary creep (stable crack extension), therefore, it cannot accurately predict creep strain at failure.

The failure criterion used for the modified 9Cr-1Mo model was that failure was considered to have occurred when the creep strain reached the experimentally determined failure strain. Since Orowan's equation cannot accurately predict tertiary creep strain, this failure criterion cannot be directly applied to 316L.

The failure criterion for 316L will replace the failure strain from the modified 9Cr-1Mo model with an effective failure strain. The effective failure strain is determined by comparing the strain-time data predicted by the model to uniaxial creep test data. An optimization process on the input parameter k_Λ and the initial condition ρ_{m0} was used to minimize the difference between the predicted strain and the experimental strain data points in the primary and secondary creep regimes. Since the experimental data is only available graphically, this process requires overlaying the predicted data onto the plotted experimental data and estimating the difference at each data point using digital image processing. In the cases where more than one set of strain data was provided for the same applied stress, the average of the two data sets was approximated. This process is pseudo-quantitative since the technique used to measure the difference between the predicted and experimental strains is not very precise. However, given the scatter in the experimental data, this imprecision is not expected to have a substantial impact on the final solution.

Once this process has been completed for all the available experimental data, the effective failure strain is defined to be the average strain at the time of experimental failure. This criteria can be applied to any combination of load and temperature, since it is a model constant.

Initial mobile dislocation density is a material constant, which has been shown in previous studies to have a negligible impact on the final strain, but a significant impact on the creep strain early in life [1]. Therefore the value of ρ_{m0} determined by the optimization process described above is considered constant for 316L.

The only remaining variable to be determined at other temperature load combinations is k_Λ. Using the previously determined constants, k_Λ can be determined for any combination of temperature and load as long as the time to failure is known. Values of k_Λ were found using a semi-

automated, quantitative optimization process to vary k_Λ until the strain at the specified failure time reached the effective failure strain.

Creep strain is not a direct function of k_Λ, rather k_Λ is a constant used to calculate the rate at which mobile dislocations are generated under the action of a load [2]:

$$\dot{\rho}_{m,gen} = \frac{M\dot{\varepsilon}}{b\Lambda} \tag{3.2}$$

$$\Lambda = \frac{k_\Lambda}{\sqrt{\rho}} \tag{3.3}$$

where b is the Burger's vector and M is the Taylor factor.

The mobile dislocation generation rate ($\dot{\rho}_{m,gen}$) is one of several terms that form a system of ordinary differential equations, which is solved in the software using an implicit numerical method. Since the analytical solution is not available, numerical methods that would typically be used to solve for k_Λ cannot be used. Instead an automated process generates a large number of strain data sets for a series of k_Λ values. Using this information, the value of k_Λ which produces the desired final strain is selected.

3.2.2. 316L Stainless Steel Material Model

Table 3.1 summarizes the material properties used in the present model for 316L stainless steel.

Table 3.1 – Material properties of 316L stainless steel at 600ºC.

Property (unit)	Value [Reference]
E (MPa)	1.48E+05 [3]
υ (-)	0.3 [3]
M (-)	3.06 [4]
b (μm)	2.58E-04 [5]
α (-)	0.3 [4]
n_g(-)	4 [6]
ε_a (mm/mm)	0.08
ρ_m (m^{-2})	1.0E+12

Properties obtained in the literature are presented with the associated citation in Table 3.1. The parameter ε_a is the relative size mismatch between the solute and solvent atoms. Its value in Table 3.1 is the ratio of the atomic radius of iron to the molar weighted average radius of the solute elements.

Uniaxial creep strain data used to obtain values of k_Λ for 316L stainless steel was taken from a series of creep tests conducted under several loads at 600ºC [7]. Figure 3.1 shows the predicted strain data selected in the optimization process described above. This data was used to determine the effective failure strain for 316L overlaid on the experimental data.

Figure 3.1 shows that the effective failure strain is about 7% strain. This data set was also used to determine the initial mobile dislocation constant and the values of k_Λ at 600ºC. Additional values of k_Λ at other temperatures improve the flexibility and robustness of the material model. Failure times from uniaxial creep tests at 550ºC [8] and 650ºC [9] were used to expand the temperature domain of k_Λ. The values computed are tabulated by corresponding temperature and stress in Table 3.2. Note that k_Λ was assumed to be constant at stresses outside of the evaluated range. In Table 3.2 the assumed values are marked with an asterisk (*).

Table 3.2 – Empirical values for constitutive model constants k_Λ for 316L stainless steel.

	550ºC	**600ºC**	**650ºC**	**Stress (MPa)**
k_Λ (-)	3.084E-03*	1.640E-04*	5.110E-02	175
	3.084E-03*	1.640E-04	1.000E-03	200
	3.084E-03*	2.019E-04	1.000E-03*	220
	3.084E-03*	2.434E-04	1.000E-03*	240
	3.084E-03	1.983E-04	1.000E-03*	260
	1.540E-02	1.983E-04*	1.000E-03*	300
	5.353E-05	1.983E-04*	1.000E-03*	320
	5.781E-05	1.983E-04*	1.000E-03*	340

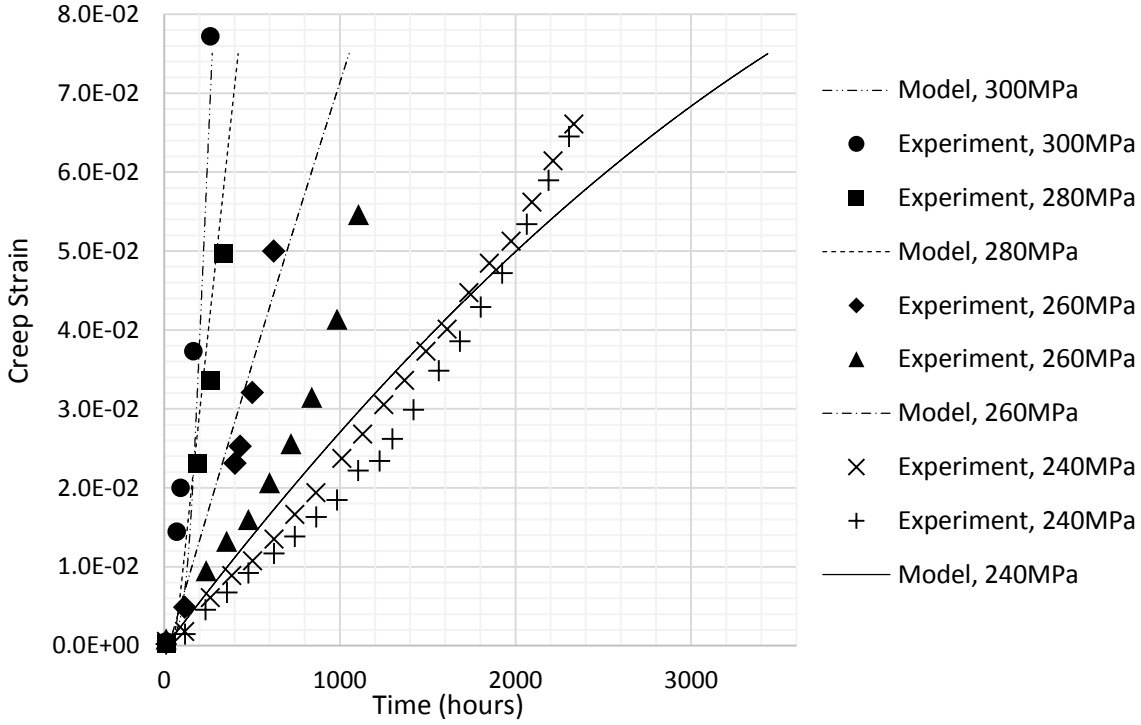

Fig. 3.1 – Comparison between predicted and experimental creep strain [23] at 600ºC.

The creep strain data predicted using these constants for the reference experimental data at 550ºC and 650ºC is shown in Figures 3.2 and 3.3. As discussed above, the predictions shown in Figures 3.2 and 3.3 can only be compared to an experimental point of failure (shown in the figure). Though the strain curves appear consistent with the curves in Figure 3.1 (which were determined from experimental data), the strains predicted by the model may be less accurate away from 600ºC.

However, based on the data shown below, the model will predict the experimental time to failure quite well. This is the quantity of interest for the present study.

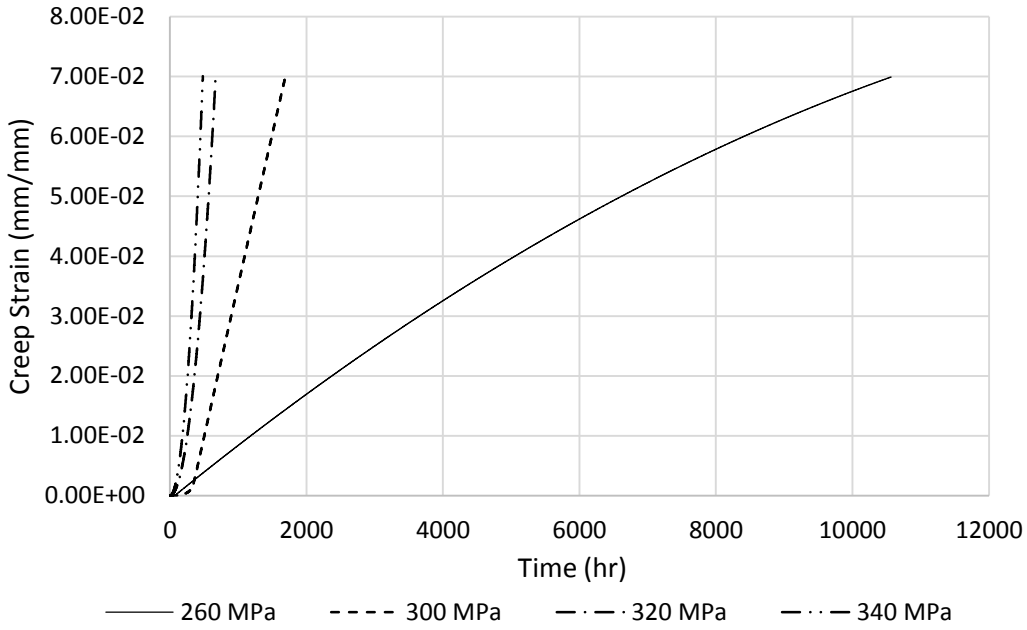

Fig. 3.2 – Predicted creep strain versus time in 316L at 550ºC.

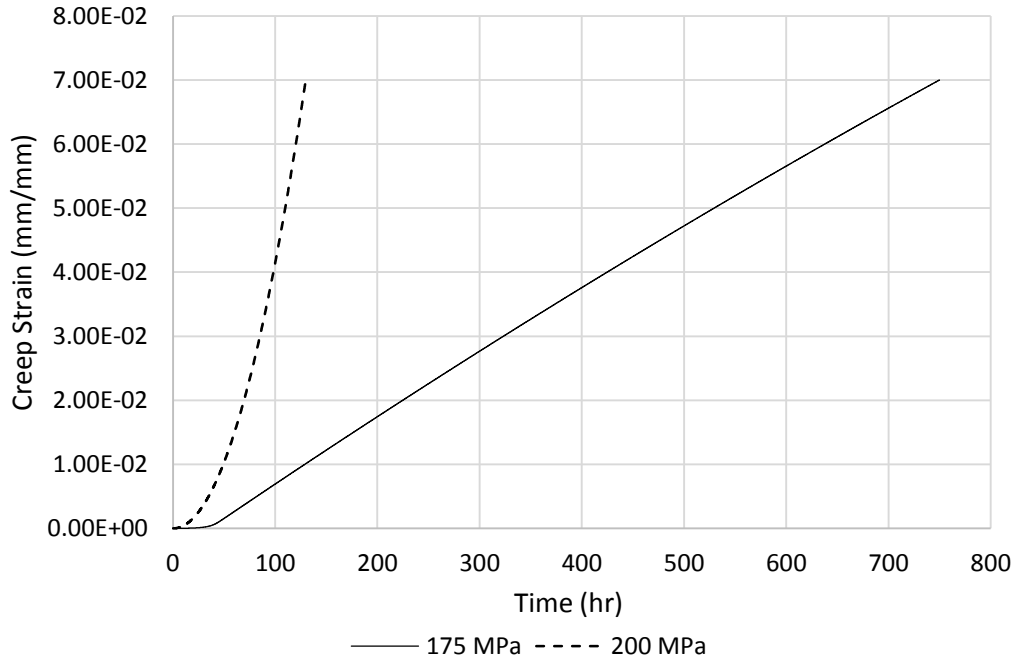

Fig. 3.3 – Predicted creep strain versus time in 316L at 650ºC.

3.2.3. Comparison to Experimental Crack Extension Data

Two sets of experimental data were modelled, one with specimens of modified 9Cr-1Mo steel [10] and the other with specimens of 316L stainless steel [11]. Material properties used for modified 9Cr-1Mo are presented in Table 3.3; material properties for 316L are presented in the previous section (see Table 3.1). Specimen geometry and loading for both data sets are presented in Table 3.4. All the tests in Table 3.4 used compact tension specimens.

Table 3.3 – Material Properties of 9Cr-1Mo Steel at 600ºC.

Property (unit)	**Value [Reference]**
σ_0 (MPa)	334.4 [9]
E (MPa)	1.25E+05 [9]
υ (-)	0.3
A (-)	1.75E+20 [12]
n (-)	8.462 [12]
ε_f^* (mm/mm)	0.18 [13]
b (μm)	2.47E-04 [8]
M (-)	3 [8]
ρ_m (m^{-2})	1.2E+14 [8]
α (-)	0.02 [8]
ε_a (mm/mm)	0.08 [8]
n_g(-)	5 [8]

Table 3.4 – Experimental specimen geometry and loading.

Experiment	**Initial crack size (mm)**	**Width (mm)**	**Thickness (mm)**	**Applied stress (MPa)**
CT1 [11]	16	32	16	108.0
CT2 [11]	17	32	16	116.69
CT3 [11]	17	32	16	110.3
CT4 [11]	17.1	32	16	102.4
CT5 [11]	17	32	16	107.7
CT6 [11]	16.8	32	16	91.3
CT7 [11]	17.1	32	16	99.1

Hyde et. al. [7] conducted creep crack extension tests in 316L stainless steel using compact tension (C(T)) specimens. Given the Chapter 2 findings regarding the empirical model, these tests were analyzed with the constitutive creep model only. Material properties and experimental

parameters were provided in Tables 3.1 and 3.4. Figure 3.4 shows the analytical results compared to the experimental data.

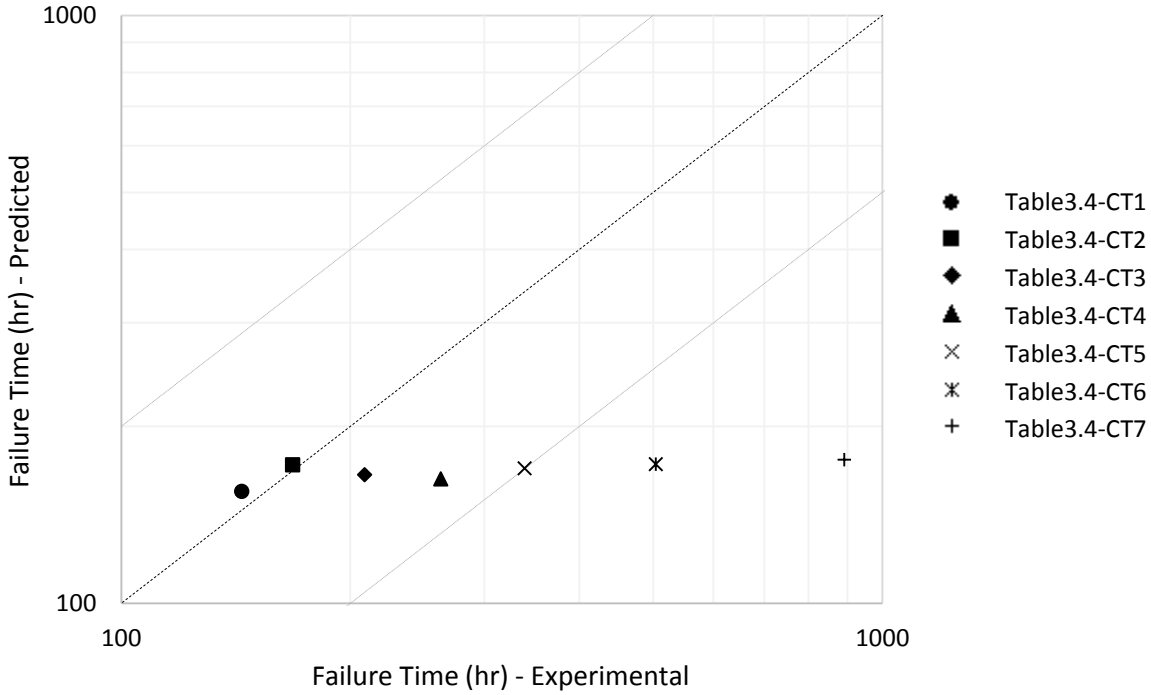

Fig. 3.4 – Predicted versus experimental failure time in specimens of 316L stainless steel

Figure 3.4 shows that some of the results seem to agree fairly well, and some do not. The model predicted similar failure times for each test regardless of applied stress. This behavior is consistent with (though more pronounced than) the comparison in Section 3.2.1 between failure times predicted by the present model and creep crack extension data in modified 9Cr-1Mo C(T) specimens [12]. Scatter in the failure times predicted by the constitutive creep model is examined and discussed in Chapter 4.

3.3. CONCLUSION

A constitutive creep material model was successfully developed from data in the open literature. Though the model predictions show some scatter relative to the experimental data (in Figure 3.4), Figures 3.1-3.3 show that the model can accurately model failure time. Additional development could extend the capability to accurately predict failure strains as well. This chapter has shown that, given a database of uniaxial creep test data, a constitutive material model such as the one developed for modified 9Cr-1Mo [12] can be developed for other materials. The scatter observed in Figure 3.4 will be discussed in Chapter 4.

3.4. REFERENCES

[1] Ennis PJ, Czyrska-Filemonowicz A. Recent advances in creep-resistant steels for power plant applications. Sadhana. 2003;28(3&4):709-30.

[2] Basirat M, Shrestha T, Potirniche GP, Charit I, Rink K. A study of the creep behavior of modified 9Cr–1Mo steel using continuum-damage modeling. International J. of Plasticity. 2012;37:95–107.

[3] Wen JF, Tu ST, Gao XL, Reddy, JN. Simulations of creep crack growth in 316 stainless steel using a novel creep-damage model. Engineering Fracture Mechanics. 2013;98:169-84.

[4] Kassner ME. Taylor hardening in five-power-law creep of metals and Class M alloys. Acta Materialia. 2004;52:1–9.

[5] Lindgren LE, Domkin K, Hansson S. Dislocations, vacancies and solute diffusion in physical based plasticity model for AISI 316L. Mechanics of Materials. 2008;40:907–19.

[6] Villechaise P, Sabatier L, Girard JC. On slip band features and crack initiation in fatigued 316L austenitic stainless steel: Part 1: Analysis by electron back-scattered diffraction and atomic force microscopy. Materials Science and Engineering. 2002;A323:377–85.

[7] Hyde CJ, Hyde TH, Sun W, Becker AA. Damage mechanics based predictions of creep crack growth in 316 stainless steel. Engineering Fracture Mechanics. 2010;77:2385–2402.

[8] Mishra M.P, Borgstedt HU, Frees G, Seith B, Mannan SL, Rodriguez P. Microstructural aspects of creep-rupture life of Type 316L(N) stainless steel in liquid sodium environment. Journal of Nuclear Materials. 1993;200:244-55.

[9] Matthew M.D, Laha K, Ganesan V. Improving creep strength of 316L stainless steel by alloying with nitrogen. Materials Science and Engineering. 2012;A535:76–83.

[10] Barker E, Lloyd GJ, Pilkington R. Creep Fracture of a 9Cr-lMo Steel. Materials Science and Engineering. 1986;84:49-64.

[11] Hyde TH. Creep crack growth in 316 stainless steel at 600ºC. High Temperature Technology. 1988;6(2):51-61.

[12] Hyde TH., Saber M, Sun W. Creep crack growth data and prediction for a P91 weld at 650ºC. International J. of Pressure Vessels and Piping. 2010;87: 721-29.

[13] Maleki S, Zhang Y, Nikbin K. Prediction of creep crack growth properties of P91 parent and welded steel using remaining failure strain criteria. Engineering Fracture Mechanics 2010;77:3035-42.

Chapter 4 – Analysis, Verification and Discussion of Model Assumptions and Constraints

4.1. INTRODUCTION

There are two foundational assumptions of the model used in the present study that contribute to the deviation between some of the predictions and the corresponding experimental data shown in Figures 2.6 and 3.4: constant stress across the creep process zone and that a C(T) specimen may be approximated by a center cracked plate. These two assumptions are implied by the use of the strip yield model.

Chapter 2 identifies a number of assumptions on which the present model is based. These assumptions will be evaluated and discussed in this chapter.

4.2. C* INTEGRAL APPROXIMATION

The NSW creep model implementation depends on the C^* integral approximation presented in Chapter 2. This approximation is based on a couple of assumptions: linear elastic section response and a load-line displacement rate approximation.

4.2.1. LINEAR ELASTIC SECTION RESPONSE

In order to validate this assumption, a finite element analysis was performed for a set experimental data in which the NSW model predictions were accurate for some outcomes and less accurate for others. The experimental data collected by Barker et. al. [1] and analyzed in Chapter 2 meets this criterion.

A quarter symmetry model of the initially un-cracked DEN(T) specimens used [1] was generated in Abaqus version 6.13-1. Since the load was applied remotely relative to the region of

interest in this test, only the section of interest was modelled and a uniform traction was applied with symmetry boundary conditions in the x and z planes (see Figures 4.1-4.3).

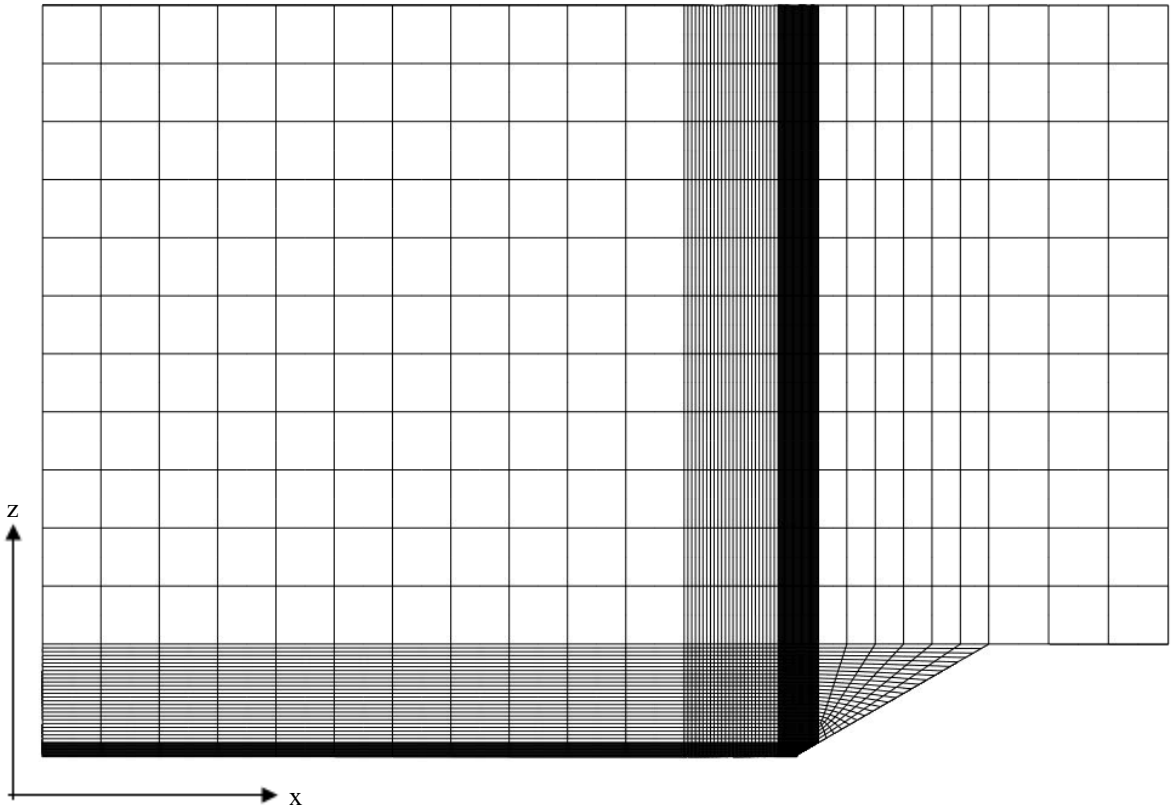

Fig. 4.1 – Entire model geometry and mesh

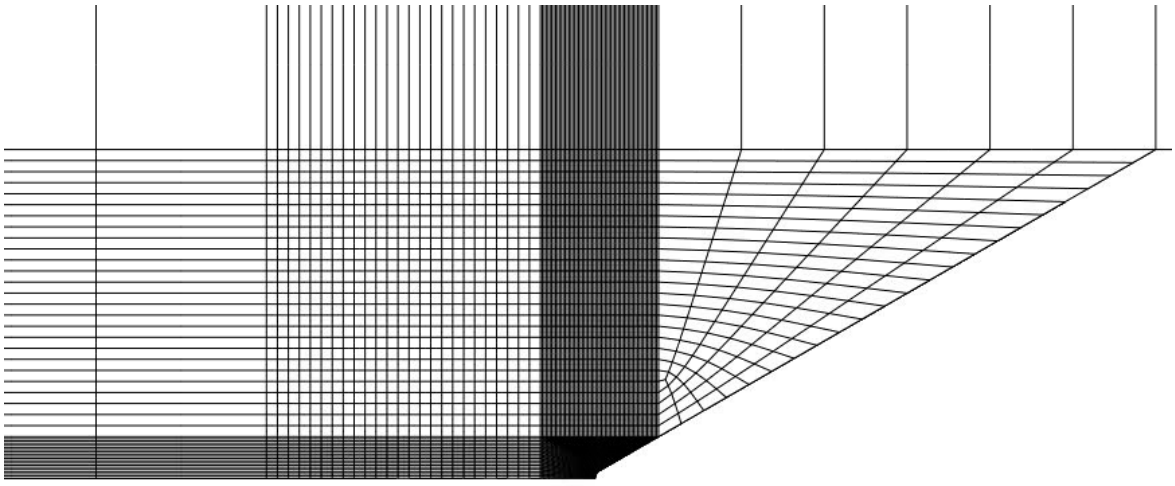

Fig. 4.2 – Close-up view, notch region mesh

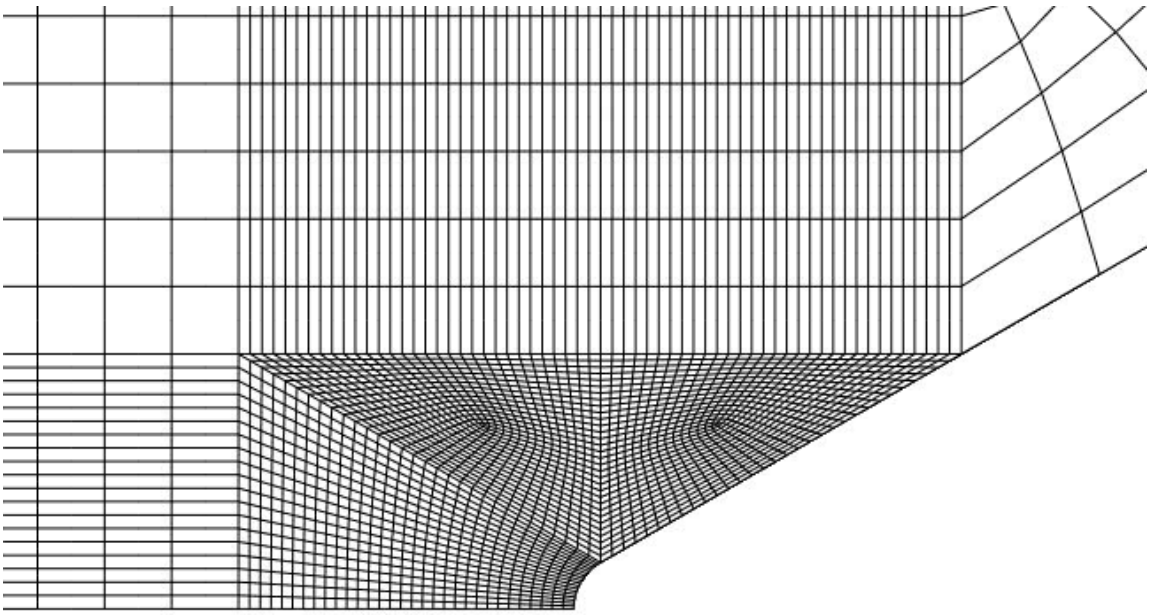

Fig. 4.3 – Close-up view, notch root region mesh

Figure 4.1 shows the model geometry and mesh; detailed close-up views of the region of interest are shown in Figures 4.2-4.3. The region of interest for this analysis is the region surrounding the notch root. Since the purpose of this study was to identify the response of the section as either linear elastic (small strains) or non-linear, Abaqus was instructed not to assume small strains (non-linear geometry option) and the iterative solver was used to obtain a solution. The entire model is meshed with continuum, 3D, quadratic, 20-node hexahedral elements with reduced integration (C3D20R) because experience has shown these elements to have excellent stability and accuracy characteristics.

All the elements in the model are 0.2 mm deep. Elements in the regions closest to the notch root are 0.005 mm on a side, the region immediately surrounding this has elements that are 0.025 mm on a side and the elements far away from the notch root are 0.4 mm on a side. Note that the mesh above the angled portion of the notch is finer than the rest of the far-field mesh. A transition region was defined over the angled portion of the notch (with elements 0.2 mm on a side) in order to ensure sufficient mesh quality in the triangular region over the notch.

The objectives of this analysis were to compare the extent of yielding between a high stress test (one which did not compare well to the empirical model) and a lower stress test (one which compared better to the empirical model) and to determine if the response of the section was linear elastic. Therefore the tests selected for the analysis had applied stresses of 195 MPa and 250 MPa corresponding to the low and high stress cases, respectively.

An elastic-plastic material model was defined in Abaqus using material properties from the literature [2] as shown in Figure 4.4.

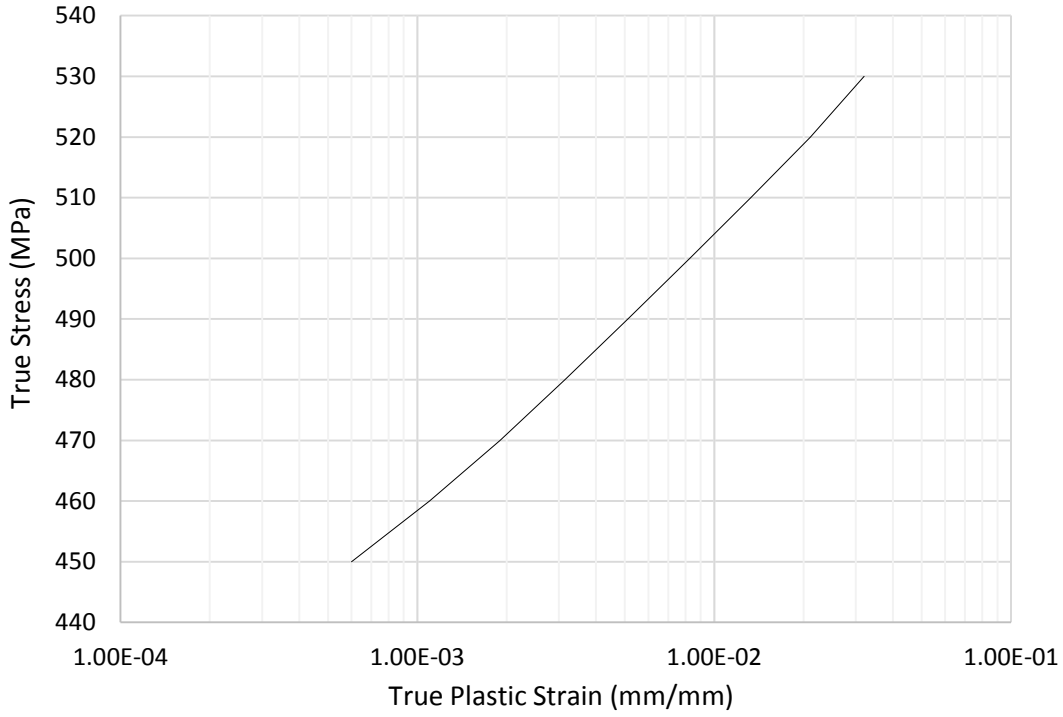

Fig.4.4 – Elastic-plastic stress-strain relationship for 9Cr-1Mo steel used in Abaqus FEA

Figures 4.5-4.6 compares the plastic strain magnitude predicted for each test and Figures 4.7 shows a comparison of the von Mises stress predicted by Abaqus through the thickness of the specimen.

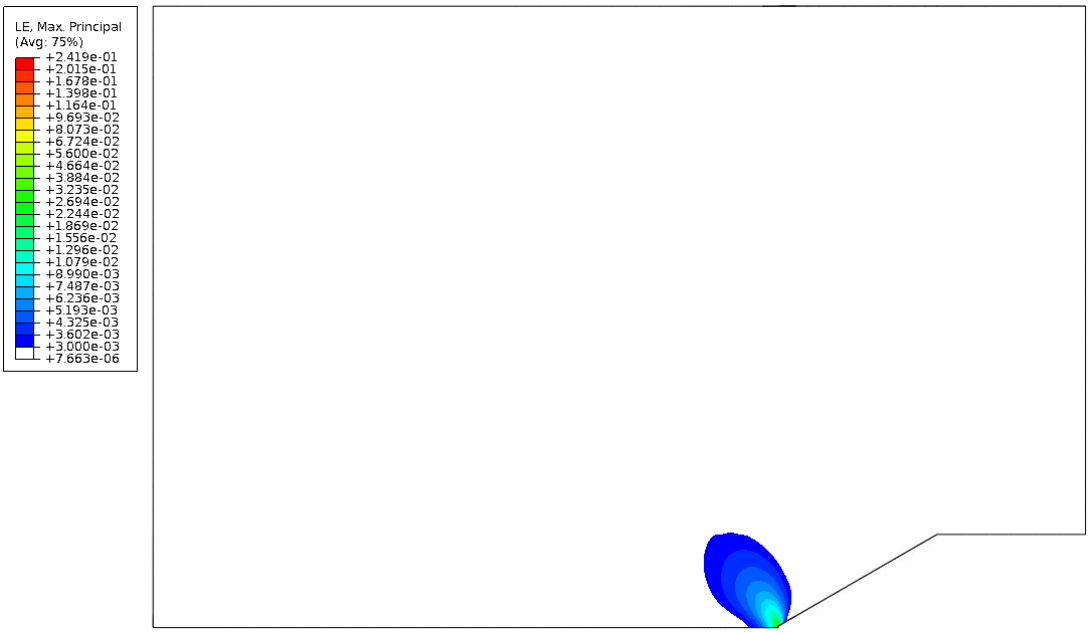

Fig. 4.5 – Plot of plastic strain magnitude with an applied stress of 195 MPa. Note that regions of purely elastic strain are white.

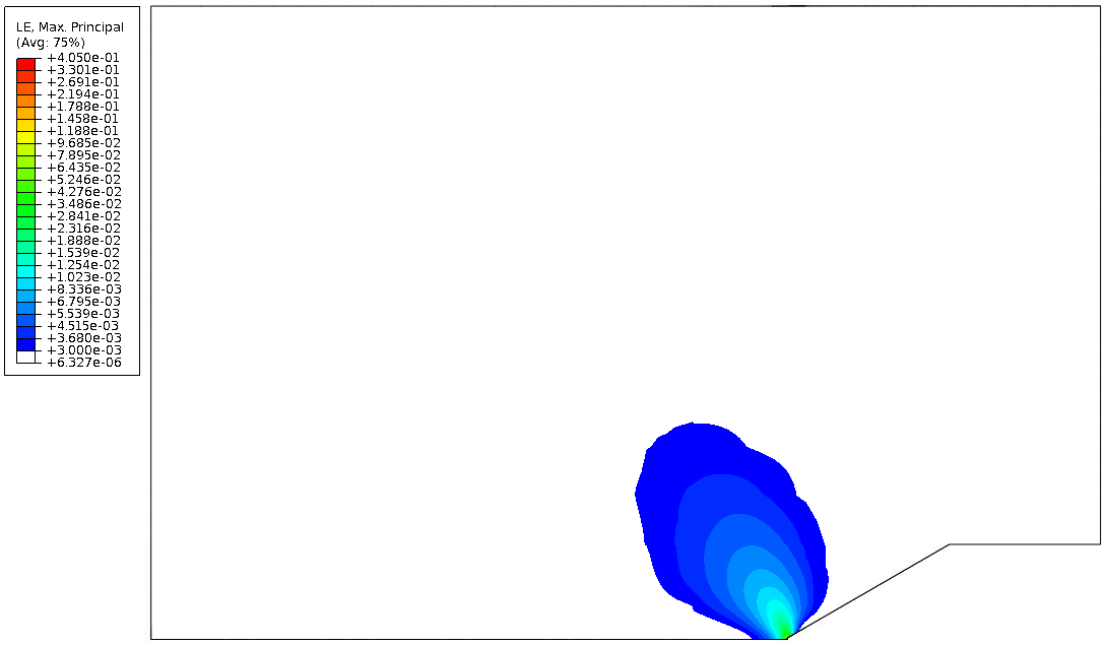

Fig. 4.6 – Plot of plastic strain magnitude with an applied stress of 250 MPa. Note that regions of purely elastic strain are white.

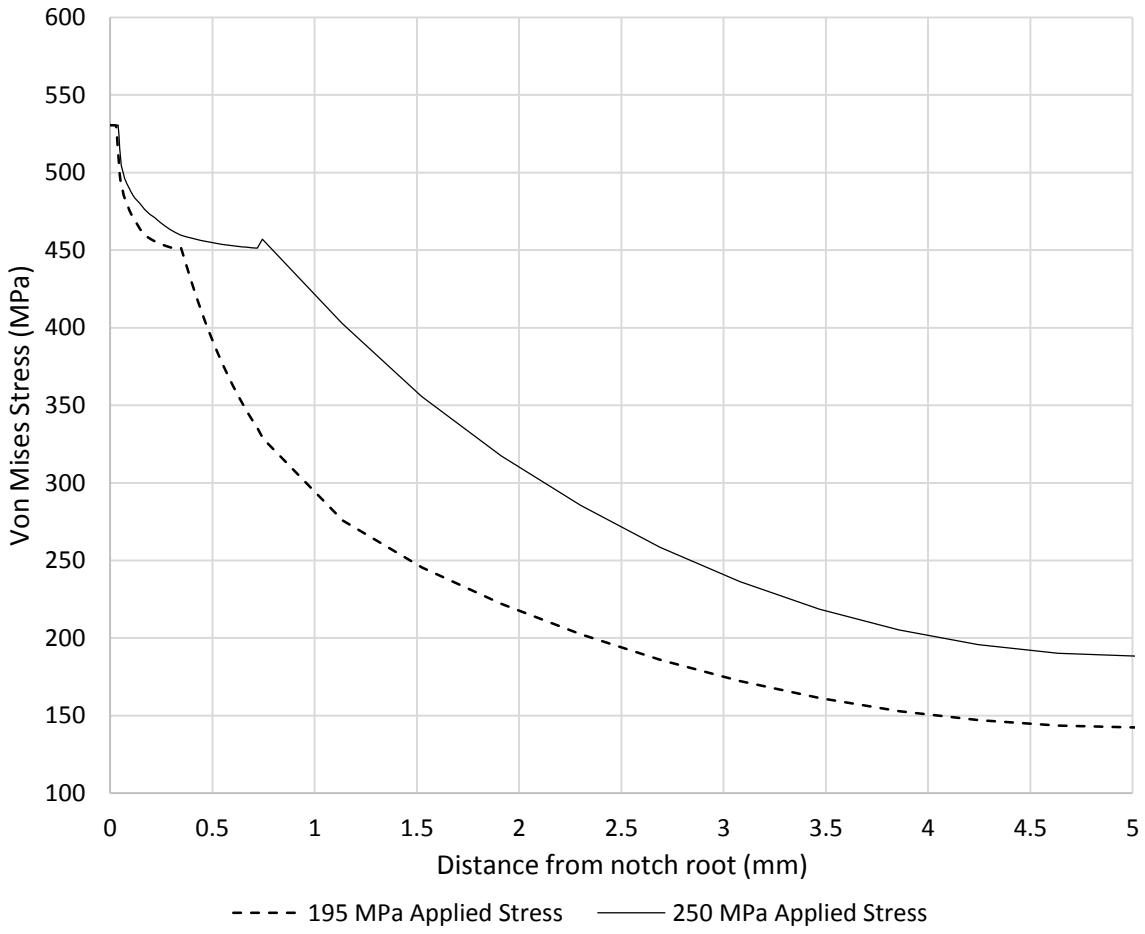

Fig. 4.7 – Plot of von Mises stress in the notch root plane for 195 MPa and 250 MPa applied stresses.

The FEA results presented in Figures 4.5-4.7 show a distinct difference in the extent and magnitude of the yielding in the section during each test. Note that, in the test at 250 MPa, about 15% of the ligament width of the DEN(T) specimen has yielded. This is consistent with the experimental findings [1] which reported substantial yielding and hardening in this region.

As mentioned above the C^* integral (like the J integral) is not restricted by small-strain or linear elastic assumptions, but the approximation of the C^* integral used in the NSW model and in the present study are based on the assumption of linear elasticity. Figures 4.5-4.7 show that even in the specimen with a 195MPa applied stress this assumption is potentially questionable, but it is

certainly not valid in the specimen with a 250 MPa applied stress. It is also worth noting that the shape of the plastic zone suggests that the assumption of essentially plane stress notch root constraint (implicit in the strip-yield model) is not accurate. The shape of the plastic zone looks qualitatively more similar to the shapes predicted by other researchers [7] under plane strain constraint than the shape predicted under plane stress constraint. These FEA results support the conclusion for why the empirical model does not accurately predict creep crack extension in specimens with large applied stresses.

Notice that there are also some discrepancies between the predictions of the constitutive model and experimental data for the specimen with a 225 MPa applied stress. Material properties for the constitutive model used in simulation were those for an applied stress of 200 MPa, since that is the highest stress for which properties were available in the literature [3]. This extrapolation of material properties is a contributing factor to the deviation between the model predictions and experimental data.

In the strip yield model, a plastic zone (creep process zone in the present study) is calculated as a distance from the crack tip. This entire region is then loaded with a constant stress, i.e., the flow stress. This process introduces potential error when used with the constitutive creep model. Since the material is assumed to be initially homogeneous (i.e., material properties have no spatial dependence) and the same load (i.e., the flow stress) is applied to the entire creep process zone, all of the yield strips in the creep process zone reach the failure strain at the same time. Therefore all of the strips are considered to fail at the same time causing the crack length to be instantaneously advanced by the length of the creep process zone. In order to illustrate this behavior, consider the evolution of crack length through life of several specimens previously discussed in Chapter 2.3.2 is shown in Figure 2.8. A few data sets of interest from Figure 2.8 are plotted in Figure 4.8.

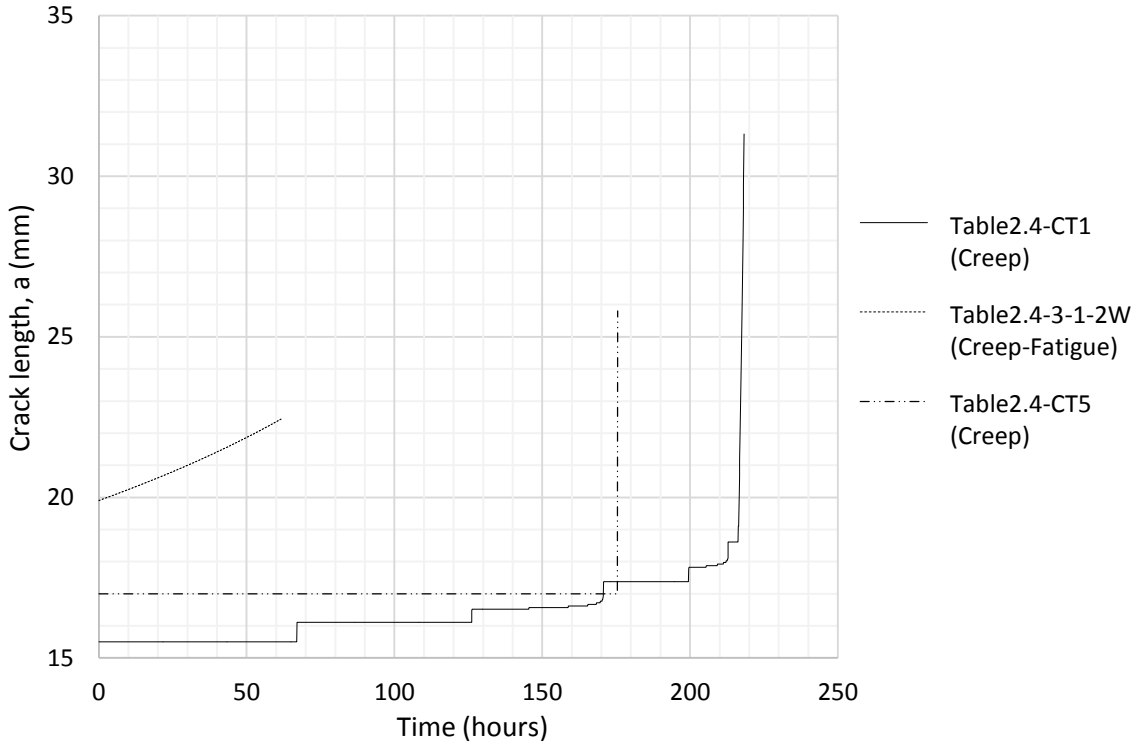

Fig. 4.8 – Change in crack length with time for creep and creep-fatigue predictions.

Notice in the data for specimen Table2.4-CT1 [4] (loaded in pure creep) there are several discontinuities in the data. These discontinuities are caused by the simultaneous failure of all the yield strips in the creep process zone, which introduces a form of discretization error if the specimen width is not much larger than the creep process zone. Creep fatigue analyses are impacted by this simultaneous failure behavior, however, the influence of this effect is mitigated in the creep-fatigue analyses because the model predicted an increment of fatigue crack growth at every time interval. Thus the crack and the creep process zone moved quasi-continuously through the material (due to fatigue crack growth) as creep strains were being calculated, which introduced sufficient variation in the creep strain field ahead of the crack that the yield strips did not all fail simultaneously. Figure 4.8 shows this effect for specimen Table2.4-3-1-2W [5] by the smooth progression of crack length through life.

Discretization error due to simultaneous failure of yield strips was likely also a factor in the creep crack extension comparisons previously presented in Section 3.2.1, Figure 2.6, however those specimens were made of modified 9Cr-1Mo steel. Due to the substantially higher flow stress (334.4 MPa compared to 260.0 MPa), the creep process zone is smaller in modified 9Cr-1Mo specimens than 316L specimens, making the effects of discretization error less obvious. This difference is shown in Figure 4.8 by comparing the data for specimen Table2.4-CT1 and Table2.4-CT5.

4.3. C(T) AS A CENTER CRACKED PLATE APPROXIMATION

Another potential source of error is the similitude argument implied by using a strip yield model (modified for a plate of finite width) to calculate the creep process zone length in a C(T) specimen. The formulation for the creep process zone length is developed from the stress intensity factor (SIF) solution. Accordingly, the stress applied to the center cracked plate model was selected so that it produced the same SIF as the prescribed load would produce in the C(T) specimen. However, since the functional dependence on crack length is not the same for both SIF, the similitude is not exact. Figure 4.9 shows a plot of normalized SIF against normalized crack length to illustrate this difference.

Some comparisons to C(T) specimens have shown better agreement than others. Therefore, the impact of this source of error on the Figure 3.4 comparison is considered to be secondary to the discretization error.

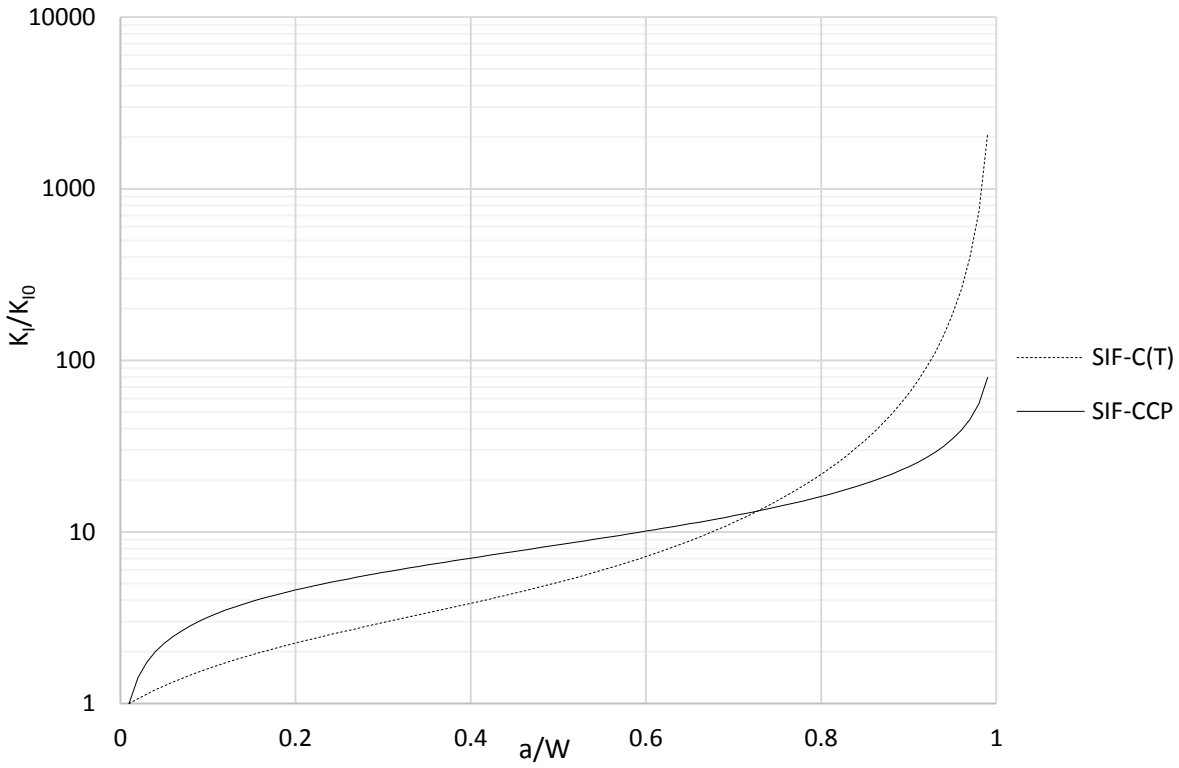

Fig. 4.9 – Comparison of the SIF for C(T) and center cracked plate (CCP)

4.4. LOAD-LINE DISPLACEMENT RATE APPROXIMATION

Previous studies have identified that the crack tip parameter and approximation method used to characterize creep crack extension can have a significant impact on the accuracy of model predictions in both modified Cr-Mo steels [9] and 316L stainless steel [6]. Haigh found that different crack tip parameters (i.e., SIF, *C** integral reference stress, etc) correlated well to creep crack extension rate for different ranges of applied stresses in the same specimen geometry [9]. This suggests that a single parameter approximation may over-simplify the material response. Wasmer, Nikbin and Webster found that the accuracy of the NSW model predictions was strongly dependent on the approximation used for *C** integral. This observation is echoed by Saxena [5], who further

suggested that reasonably accurate C^* predictions were impractical without developing an empirical load-line displacement rate correlation for the experimental conditions of interest.

The present model uses an approximation for load-line displacement rate based on the small strain linear elasticity assumption and the assumption that the only time varying source of strain is creep. In consideration of the observations of the above researchers, this approximation is likely a contributing factor to the scatter in the NSW model creep crack extension predictions.

4.5. PLANE STRESS CONSTRAINT

In general, plane stress crack tip constraint is considered to apply to cracks in specimens where the thickness is small compared to the other dimensions in the problem. In these conditions, the out-of-plane stress is assumed to be negligible due to the proximity of the traction-free surfaces. However, both analysis [7] and testing [8] have shown that the plane stress assumption does not predict the plastic zone size accurately for many test thin specimens. Figure 4.10 [7] plots the out-of-plane stress predicted by finite element analysis of the crack tip region normalized by geometric dimensions. In order for the plane stress assumption to accurately predict the plastic zone size, the triaxiality should be approximately zero at all distances from the crack tip. Figure 4.10 [7] illustrates why the plane stress assumption in the strip-yield model will introduce non-trivial error into the model predictions for most test specimens: the triaxial stress is not trivial for a considerable distance into the creep process zone. Based on Figure 4.10, the creep process zone in test specimens studied in Chapters 2 and 3 are expected to experience some combination of plane stress and plane strain constraint.

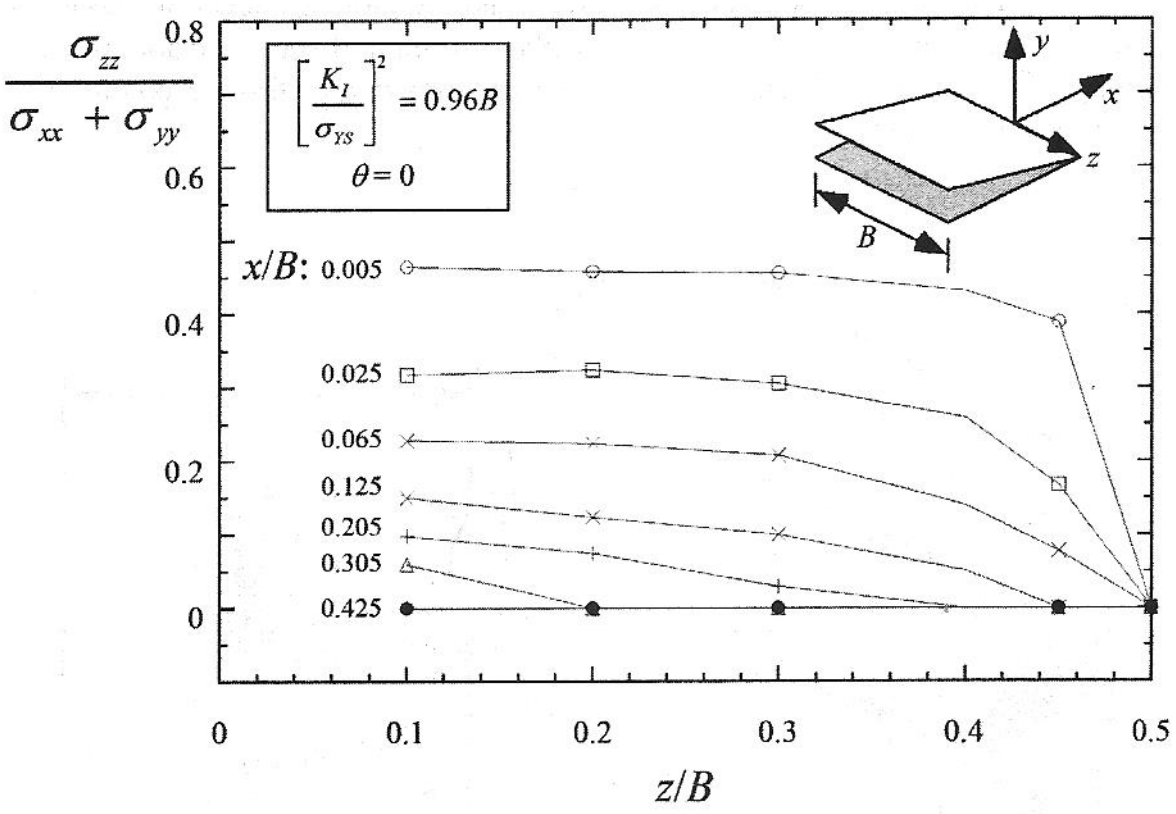

Fig. 4.10 – Triaxial stress versus normalized specimen geometry near a crack tip.

Newman et. al. developed an empirical constraint parameter for the strip-yield model. This constraint adjustment factor showed good agreement to fatigue crack growth test data [8], but was not implemented in the present model due to practical limitations.

4.6. CONCLUSION

The strip yield model is used in the present model to represent the crack tip stress field in the creep process zone. The strip-yield model and the NSW empirical creep model are based on several foundational assumptions which are used to approximate the physical behavior. Though models provide a reasonable approximation of the experimental data, the assumptions behind them introduce

non-trivial scatter into the model predictions. This effect must be considered when interpreting the results of the Chapters 2 and 3 comparisons to experimental data.

4.7. REFERENCES

1[1] Barker E, Lloyd GJ, Pilkington R. Creep Fracture of a 9Cr-lMo Steel. Materials Science and Engineering. 1986;84:49-64.

[2] Chouldhary BK, Christopher J, Rao Palaparti DP, Isaac Samual E, Matthew, MD. Influence of temperature and post weld heat treatment on tensile stress–strain and work hardening behavior of modified 9Cr–1Mo steel. Materials and Design. 2013;52:58–66.

[3] Basirat M, Shrestha T, Potirniche GP, Charit I, Rink K. A study of the creep behavior of modified 9Cr–1Mo steel using continuum-damage modeling. International J. of Plasticity. 2012;37:95–107.

[4] Hyde TH., Saber M, Sun W. Creep crack growth data and prediction for a P91 weld at 650ºC. International J. of Pressure Vessels and Piping. 2010;87: 721-29.

[5] Narasimhachary SB, Saxena A. Crack growth behavior of 9Cr-1Mo (P91) steel under creep–fatigue conditions. International J. of Fatigue. 2013;56:106–13.

[6] Wasmer K, Mikbin KM, Webster GA. Influence of reference stress formulae on creep and creep-fatigue crack initiation and growth prediction in plate components. International J. Pressure Vessels and Piping. 2010;87:447-56.

[7] Anderson TL. Fracture Mechanics: Fundamentals and Applications. Third ed. Boca Raton (FL): CRC Press; 2005.

[8] Newman, Jr. JC. A Crack Closure Model for Predicting Fatigue Crack Growth under Aircraft Spectrum Loading. Methods and Models for Predicting Fatigue Crack Growth under Random Loading, ASTM STP 748. Chang JB, Hudson CM, Eds. Philadelphia: American Society for Testing and Materials; 1981:53-84.

[9] Haigh JR. The Mechanisms of Macroscopic High Temperature Crack Growth. Part I: Experiments on Tempered Cr-Mo-V Steels. Material Science Engineering 1975;20:213–223.

Chapter 5 – General Conclusions & Recommendations for Future Research

5.1. DISCUSSION

The present study presented a strip yield creep-fatigue model and compared crack growth predictions to test data over a wide range of temperatures, stresses and materials. A constitutive creep material model was developed for 316L stainless steel, a ductile steel popular for high temperature applications, especially in corrosive environments. The model was successfully compared to experimental data from modified 9Cr-1Mo steel and 316L. A few conclusions can be drawn from these studies:

1. The constitutive creep model consistently performs better than the NSW model for predicting creep and creep-fatigue crack extension.
2. Given a database of uniaxial creep test data, a constitutive material model such as the one developed for modified 9Cr-1Mo [1] can be developed for other materials.
3. Due to the assumptions used to develop the strip-yield model, model predictions are expected to show some scatter. This scatter is observed in the Chapters 2 and 3 data.

Due to the limited availability of creep-fatigue experimental data in the literature, only one creep-fatigue comparison was made (in Chapter 2). As a result, this study does not provide much insight into the accuracy or suitability of the fatigue crack growth model used (Paris law). Similar to the strip yield model, this method was implemented because it is simple and has been shown to give reasonably accurate results in a variety of situations. However, future research should consider alternative methods for predicting fatigue crack growth. Given that the creep model implemented is based on a constitutive equation [1], a similar model for fatigue crack growth would be desirable.

In Chapter 3, a new material model for AISI 316L stainless steel was developed. This showed that the constitutive creep model had applications to materials other than modified 9Cr-1Mo. Future research should continue to develop new material models and refine the existing ones. This effort would probably require a non-trivial uniaxial creep test program to assemble the data needed to produce and improve material models.

Chapters 2 and 3 compared model predictions to test data from the open literature. This is appropriate for the initial model development phase of research since test programs are expensive. The present model has shown promising comparisons to test data from the literature, so future research should implement a test program to collect creep-fatigue data for a variety of loads, geometries and materials.

Chapter 4 verified and discussed assumptions behind the present model the impact of these assumptions on the results of Chapters 2 and 3. Future research should implement the present creep-fatigue model as a user-defined subroutine in a finite element solver. By providing more precise applied stresses at each point in the specimen, this would mitigate the discretization, similitude and constraint error from the strip yield model and tie the present model directly with practical tools used for many types of engineering analysis.

5.2. REFERENCES

[1] Basirat M, Shrestha T, Potirniche GP, Charit I, Rink K. A study of the creep behavior of modified 9Cr–1Mo steel using continuum-damage modeling. International J. of Plasticity. 2012;37:95–107.